

# MAPPING COSMOLOGICAL OBSERVABLES TO THE DARK KINETICS

SERGEI BASHINSKY

Theoretical Division, T-8, Los Alamos National Laboratory, Los Alamos, NM 87545  
sergeib@lanl.gov

*Draft version August 27, 2021*

## ABSTRACT

We study systematically which features in the cosmic microwave background (CMB) and large-scale structure (LSS) probe various inhomogeneous properties of the dark sectors (including neutrinos, dark matter, and dark energy). We stress, and quantify by simple formulas, that the primary CMB anisotropies are very susceptible to the gravitational potentials during horizon entry, less at recombination. The CMB thus allows us to scan  $\Phi + \Psi$  and the underlying dark kinetics for all redshifts  $z \sim 1 - 10^5$ . LSS, on the other hand, responds strongest to  $\Phi$  at low redshifts. Dark perturbations are often parameterized by the anisotropic stress and effective sound speed (stiffness). We find that the dark anisotropic stress and stiffness influence the visible species at the correspondingly early and late stages of horizon entry, and affect stronger respectively the CMB and LSS. The CMB yet remains essential to probing the stiff perturbations of light neutrinos and dark energy, detectable only during horizon entry. The clustering of dark species and large propagation speed of their inhomogeneities also map to distinctive features in the CMB and LSS. Any parameterization of the signatures of dark kinetics that assumes general relativity can effectively accommodate any modified gravity (MG) that retains the equivalence principle for the visible sectors. This implies that formally the nonstandard structure growth or  $\Phi/\Psi$  ratio, while indicative, are not definitive MG signatures. The definitive signatures of MG may include the strong dependence of the apparent dark dynamics on visible species, its superluminality, and the nonstandard phenomenology of gravitational waves.

*Subject headings:* cosmology: theory — cosmic microwave background — large-scale structure of universe — dark energy — modified gravity

## 1. INTRODUCTION

Galactic and cluster dynamics, cosmic structure, type Ia supernovae, the cosmic microwave background (CMB), and the primordial abundances of light elements provide solid evidence that dark sectors constitute a significant energy fraction of the universe at any accessible redshift  $z \lesssim 10^{10}$ . At all corresponding cosmological epochs the nature of abundant dark species, coupled to photons and baryons only by gravitation, is partly or entirely uncertain.

The mainstream analyses of cosmological data usually assume the minimal neutrino sector, non-interacting cold dark matter (CDM), and dark energy represented by a canonical scalar field (quintessence). These assumptions are reasonable for interpreting the available data, yet none of them can be taken for granted. For example, new light weakly interacting particles commonly appear in high-energy models. In some models, even the standard neutrinos recouple to each other or to additional light fields (Chacko et al. 2004, 2005; Beacom et al. 2004; Okui 2005; Grossman et al. 2005) at redshifts at which the decoupled component of radiation gravitationally affects the CMB and cosmic structure (Hu & Sugiyama 1996; Bashinsky & Seljak 2004; Hannestad 2005; Bell et al. 2006). Various alternatives to cold dark matter have been suggested as well. These include warm dark matter (Blumenthal et al. 1982; Olive & Turner 1982), self-interacting dark matter (Carlson et al. 1992; de Laix et al. 1995; Spergel & Steinhardt 2000), or modified gravity (Milgrom 1983; Bekenstein 2004; Skordis et al. 2006; Dodelson & Liguori 2006). The viability of such scenarios remains an intriguing question. Quintessence models are convenient for quantitatively constraining dark energy parameters by data. Yet quintessence is not readily motivated by particle physics, where it is difficult to naturally achieve the required shallowness of the field potential. On the other hand, many alternatives have been

proposed whose inhomogeneous kinetics, and hence cosmological signatures, *cannot be mimicked by quintessence with any background equation of state  $w(z)$* . (For a comprehensive review of dark energy models see, e.g., Copeland et al. 2006).

Fortunately, cosmological observations themselves can test these assumptions by revealing not only the dark species' mean density and pressure but also the kinetics of their inhomogeneities. The goal of this paper is to map various inhomogeneous kinetic properties of the dark sectors (or deviations from Einstein gravity) to the observable characteristics of CMB and cosmic structure. Dark species influence the visible matter by affecting both the background expansion and metric perturbations. Of the two mechanisms, the perturbations, albeit demanding better statistics for useful constraints, encode many more independent clues about the dark universe by offering *new information at every spatial scale  $k$* . The following three examples show the importance of this information, absent in the background equation of state  $w(z)$ .

### 1.1. Examples of the value of dark perturbations

#### *Nature of dark energy*

The first example is the most challenging problem in today's cosmology—the nature of dark energy. The constraints on the dark energy background equation of state  $w \equiv p_{\text{de}}/\rho_{\text{de}}$  are tightening around the value  $-1$ , consistent with a cosmological constant. Analyses that combine the current data from the CMB, large scale structure (LSS), Lyman- $\alpha$  forest, and supernovae, already constrain the deviation of  $w$  from  $-1$  for flat models better than to 10% (Spergel et al. 2006; Seljak et al. 2006; Tegmark et al. 2006, and others.) Whether or not future observations continue to converge on  $w = -1$ , the dynamics of perturbations will be crucial in elucidating the nature of cosmic acceleration.

Even if  $w(z) \equiv -1$  at low redshifts, this does not neces-

sarily imply a cosmological constant. Certain models (e.g. Fardon et al. 2006) predict that  $w \equiv -1$  at the present epoch, yet the dynamics of perturbations differs at high redshifts. Contrary to common belief, it is even conceivable that  $w \approx -1$  yet low-redshift perturbations deviate from those in the  $\Lambda$ CDM model. On the other hand, if  $w \neq -1$  then perturbations of dark energy in the inhomogeneous metric are unavoidable. (Even if dark energy appears unperturbed in one spacetime slicing, its perturbations for  $w \neq -1$  are necessarily nonzero in any different slicing.) Exploring the perturbations' properties, specifically the properties considered in this paper, will then become pivotal to establishing the nature of dark energy.

### Density of dark radiation

The current observations of CMB temperature and polarization, including the WMAP 3-year results (Hinshaw et al. 2006; Page et al. 2006), when combined with the SDSS galaxy power spectrum (Tegmark et al. 2004; Eisenstein et al. 2005), with or without Ly- $\alpha$  forest data, prefer enhanced neutrino density. Seljak et al. (2006) report  $N_\nu = 5.3^{+2.1}_{-1.7}$  at  $2\sigma$ , disfavoring the standard value  $N_\nu = 3.04$  at  $2.4\sigma$ . The WMAP team in its latest analysis (Spergel et al. 2006) likewise concludes that from the WMAP3 and SDSS data  $N_\nu = 7.1^{+4.1}_{-3.5}$ . A similar preference for high  $N_\nu$  by the WMAP3 and SDSS data is seen by Cirelli & Strumia (2006), although not by Hannestad & Raffelt (2006).

While neutrinos noticeably speed-up the background expansion in the radiation era, by itself this leads to almost no observable cosmological signatures (Hu et al. 1999; Bashinsky & Seljak 2004; Bashinsky 2004), given the freedom of a compensating adjustment of matter density  $\Omega_m h^2$  (Bowen et al. 2002) and primordial helium fraction  $Y_p$  (Bashinsky & Seljak 2004).

This degeneracy is broken by the differences in the evolution of streaming neutrino perturbations and of the acoustic waves in the photon-baryon fluid. It is also broken by independent constraints on the helium fraction. Various signatures of neutrinos that then appear remain partly degenerate with nuisance parameters, such as the dark energy equation of state or the normalization and tilt of the primordial power. Yet these signatures and the constraints on  $N_\nu$  with the correspondingly different experiments have rather incomparable degree of robustness (Bashinsky & Seljak 2004).

The preference of WMAP3+SDSS data for an enhanced neutrino density could be due to the physical excess of matter power over CMB power, expected for higher density of freely streaming particles (Hu & Sugiyama 1996; Bashinsky & Seljak 2004). Yet other explanations, e.g., incomplete treatment of recombination or insufficient accuracy of bias modeling, also cannot be definitely excluded.

In addition to increasing the ratio of matter to CMB power, freely streaming neutrinos shift the phase of CMB acoustic oscillations (Bashinsky & Seljak 2004). The phase-shift signature is very robust to systematic uncertainties and will become the primary discriminative mechanism for the near-future tight CMB constraints on neutrino density (Lopez et al. 1999; Bowen et al. 2002; Bashinsky & Seljak 2004; Perotto et al. 2006), e.g.  $\sigma(N_\nu) \sim 0.2 - 0.3$  expected from the Planck mission<sup>1</sup>. It can provide decisive evidence for the excess of streaming relativistic particles or rule this possibility out.

### Nature of dark radiation

If there is a true excess of energy density in the radiation era, at least three alternatives for non-standard dark radiation are possible: relic decoupled particles, self-interacting particles (Chacko et al. 2004, 2005; Beacom et al. 2004; Hannestad 2005), or a tracking classical field (Ratra & Peebles 1988; P. Ferreira, M. Joyce 1997; Zlatev et al. 1999). The perturbations of dark radiation propagate differently in all of these scenarios. As follows from this work, this in principle allows their experimental discrimination.

#### 1.2. Questions not answered by black-box computations

For a particular cosmological model it is generally straightforward to calculate linear power spectra and transfer functions with standard codes, if necessary, modified to include new dynamics. Despite this, numerical calculations have limited usefulness for exploring the signatures of new physics: First, for typical models, with close to ten unknown nuisance parameters, it is often intricate to establish numerically which of the observable signatures of the new physics cannot be compensated by parameter adjustments. While only such signatures are the true discriminators of the physics in question, they may be tiny and easily overlooked among large yet degenerate effects. Moreover, for every extended parameterization of the nuisance effects as well as for any additional constraining experiment, a new numerical analysis is required.

Equally importantly, a numerical black-box computation does not answer which aspects of a model are responsible for its observable signatures. This obscures the separation of the physical facts that are backed by observations from the models' features that are believed true yet are untested.

#### 1.3. Approach, outline, and conventions

The approach of this paper is to explicitly track the evolution of gravitationally coupled inhomogeneities of the visible and dark species. This allows us to identify which observables are affected by which of the various properties of the dark kinetics. Importantly, this approach also reveals the mechanisms behind the sensitivity of cosmological observables to various dark properties. Establishing the mechanism allows us to judge more intelligently the robustness of cosmological constraints, particularly, to know when this mechanism may fail or produce a different outcome.

As we will see soon, there is an important subtlety in performing such identifications. To decipher the signatures of the dark kinetics, it is essential to address the gravitational interaction of perturbations during *horizon entry*. Then and only then perturbations of all abundant dark species are gravitationally imprinted on the visible species without suppression. The suppression of the impact of the species' energy overdensity  $\delta\rho/\rho$  on the metric on subhorizon scales is evident from the Poisson equation

$$\Phi = -k^{-2}4\pi G a^2 \delta\rho \sim (\mathcal{H}/k)^2 \delta\rho/\rho, \quad (1)$$

where  $k$  is the (comoving) wavevector of a perturbation mode and  $\mathcal{H}$  is the expansion rate (in conformal time). The impact of the species' velocities is suppressed even more [by  $(\mathcal{H}/k)^3$ , c.f. eq. (11).] At horizon entry, on the other hand, the factor  $\mathcal{H}/k$  approaches unity and does not cause suppression. In particular, only during the horizon entry are the visible species influenced by the perturbations of dark radiation and dark energy,

<sup>1</sup> <http://www.rssd.esa.int/Planck>

for which the Jeans length is expected to be close to the horizon size.

Numerous authors (e.g., Press & Vishniac 1980; Bardeen 1980; Ma & Bertschinger 1995) have pointed out considerable freedom in representing the inhomogeneous evolution on the scales of the order of and exceeding the Hubble scale. This freedom is due to, literally, an infinite number of possibilities for coordinate gauges, as well as for the variables (even the gauge-invariant ones) that can parameterize large-scale perturbations. In principle, this descriptive freedom could introduce ambiguity in relating observable features with specific physical mechanisms that operate on large scales. Moreover, such relations indeed differ among the authors who use apparently dissimilar while formally equivalent descriptions—differ substantially for some pronounced and important for constraints features.

We argue in Sec. 2 that, as far as the observable impact of dark dynamics is concerned, there is little room for ambiguities. A well defined distinction can be drawn between an apparent connection “dynamical cause  $\rightarrow$  observable effect” that is a descriptive artifact or that is an objective causal relation. We will also see that in certain formalisms, which exist and can be distinguished by simple criteria, the physical microscopic properties that characterize species at a particular time influence the apparent large-scale perturbations *at the same time*. Such formalisms markedly simplify mapping of the characteristics of cosmological observables to the responsible microscopic dark kinetics.

In the subsequent sections we do such a mapping for the CMB temperature power spectrum and LSS transfer functions. In Sec. 3 we discuss the general features of the primary probes of inhomogeneous cosmological dynamics. We also give dynamical equations to be used further to quantify the CMB and matter response to dark parameters. In Sec. 4 we review various general parameterizations of potentially accessible information about the properties of dark sectors. We consider the parameterizations of the metric, of dark densities and stresses, and of internal dark dynamics. Sec. 5 is central to our study. In this section we identify the characteristics of the CMB and cosmic structure that reveal such general properties of dark species as anisotropic stress, stiffness, clustering, and propagation of inhomogeneities. In Sec. 6 we study the specifics of cosmologies with modified gravity and discuss how modified gravity can be distinguished observationally. Our main results are summarized in Sec. 7 and its Table 1.

Throughout the paper, distances will be measured in comoving units. Evolution will usually be described in conformal time  $d\tau = dt/a$ , where  $a$  is the cosmological scale factor and  $dt$  is proper background time. Overdots denote derivatives with respect to the conformal time, and  $\mathcal{H} \equiv \dot{a}/a = Ha$  gives the Hubble expansion rate in conformal time.

## 2. IS MAPPING OF LARGE-SCALE DYNAMICS TO OBSERVABLES UNAMBIGUOUS?

Except for Sec. 6, we will consider models in which dark and visible sectors couple by standard Einstein gravity. These models correspond to a local action  $S = \int d^4x \sqrt{-g} \mathcal{L}$  with  $\mathcal{L} = \mathcal{L}_{\text{dark}} + \mathcal{L}_{\text{vis}} + \mathcal{L}_{\text{grav}}$ , where the dark degrees of freedom are represented by the Lagrangian density  $\mathcal{L}_{\text{dark}}$ , the visible ones by  $\mathcal{L}_{\text{vis}}$ , and the gravitational ones by  $\mathcal{L}_{\text{grav}} = (16\pi G)^{-1}R$ . In agreement with observations, we assume that the large-scale evolution can be presented as a mildly perturbed Friedmann-Robertson-Walker (FRW) expansion. For this section only, we clock

the evolution by the number of  $e$ -foldings  $N \equiv \ln a$ , tractable through local matter density or CMB temperature.

Let  $[N_1, N_2]$  be an evolution interval in the past. Consider a class,  $M_{12}$ , of all conceivable models with same  $\mathcal{L}_{\text{vis}}$  that:

- (i) evolve identically for  $N < N_1$ ;
- (ii) during the interval  $[N_1, N_2]$  possibly differ in the microscopic laws of their dark, but not visible, dynamics; and
- (iii) by  $N = N_2$  have identical distribution of the dark species (in some non-degenerate measure) among all  $M_{12}$  models.

By  $N = N_2$ , the distributions of the visible species among these models will generally differ: The visible species would generally be gravitationally affected earlier by the model-specific evolution in the dark sectors.<sup>2</sup>

Given a quantity  $P$  that characterizes internal dark dynamics and an observable  $O$ , the following may be true: Regardless of the value of  $P$  during the interval  $\Delta N_{12} \equiv [N_1, N_2]$ , all the models in the above class  $M_{12}$  have the same observed value of  $O$ . Then it is natural to say that the observable  $O$  is *not sensitive* to the considered dynamical property  $P$  in the interval  $\Delta N_{12}$ .

In linear order, this applies to the effects of any dark property  $P$  on any observable  $O$  that depends only on the perturbations that were superhorizon during  $\Delta N_{12}$ . Wands et al. (2000) showed that perturbations in several gravitationally coupled fluids can be described by variables which during superhorizon evolution (for non-decaying modes) are time-independent in each of the individual fluids.<sup>3</sup> This result can be extended beyond multifluid models to any sector that is perturbed (internally) adiabatically, i.e., is homogeneous in at least some coordinates (Bashinsky & Seljak 2004). In other words, linear perturbations encode no information about the microscopic properties that characterized the dark universe when these perturbations were superhorizon.

The abundances and kinetic properties that dark species have *since horizon entry* do influence the observed CMB or matter perturbations. However, because of the aforementioned freedom in representing the evolution of large-scale inhomogeneities, in many formalisms (including the most popular ones), the properties characterizing the dark species at horizon entry affect the apparent perturbations of the CMB or matter long before or after the entry. This can mislead one into viewing an observable feature as a probe of an entirely unrelated epoch and/or physical process. This source of existing and potential new misassignments can be eliminated systematically and naturally as follows.

The impact of local dark dynamics on perturbations of visible species will appear concurrent with the underlying microscopic dark physics in any formalism which has the following two properties (Bashinsky 2006):

<sup>2</sup> Even the dark species in the  $M_{12}$  models may not be perturbed identically at  $N_2$  in terms of every measure. On large scales the quantification of dark perturbations by a different measure can depend on the perturbations of visible species and the metric. We require only that the dark perturbations are the same in at least one non-degenerate measure.

<sup>3</sup> Linde & Mukhanov (2006) noted that under certain conditions, which may exist, e.g., during reheating, *gravitational* decays of species into another type of species may mix the superhorizon perturbations in different sectors. Such decays are, nevertheless, negligible for the post-BBN evolution studied in this paper.

- I. Perturbations are frozen on superhorizon scales.
- II. Perturbations evolve by the equations of the FRW metric whenever the geometry is unperturbed.

We imply that the description of gravity in these formalisms reduces to the Newtonian one in the weakly perturbed metric on subhorizon scales. This is easily achieved, e.g., by parameterizing metric inhomogeneities by the gravitational potentials of the Newtonian gauge (Mukhanov et al. 1992; Ma & Bertschinger 1995).

Then the apparent linear impact of dark species on observables will be found to be identical in any description with properties I and II: This impact is practically unambiguous for the evolution of perturbation modes after horizon entry; the apparent perturbations do not evolve at all prior to the entry by condition I. Therefore, these descriptions could differ only by the changes of perturbations during horizon entry. It is straightforward to argue (Bashinsky 2006) that there are no such differences in linear theory among the formalisms that satisfy I and II.

One such particular, natural and simple, formulation of the full linearly perturbed Einstein-Boltzmann cosmological dynamics was described in Bashinsky (2006). This formulation is based on *canonical* coordinate variables. The canonical variables for perturbations of phase-space distributions or radiation intensity were considered in the past (e.g., Chandrasekhar 1960; Durrer 2001) but have not become mainstream in the present cosmology. In addition to the demonstrated more direct connection of large-scale evolution to microscopic kinetics of cosmological species, this formulation has several technical advantages over popular alternatives, most of which consider perturbations of proper quantities. It is used in the analysis that follows.

### 3. PROBES

Following the standard route, we separate the effects of dark sectors on the metric into the contributions to the background geometry and to metric inhomogeneities. The background geometry is fully described by the Hubble expansion rate as a function of redshift and by possible global curvature. It is constrained by a variety of “geometrical” probes, e.g., the luminosity-redshift relation for type Ia supernovae or the angular size of the acoustic features in the power spectra of the CMB and matter. In this paper we focus on extracting the potentially much richer information about the dark dynamics that is contained in the metric inhomogeneities. This information is to be inferred from the imprints of the metric inhomogeneities on such various observables as the CMB, galaxy distributions, lensing shear, quasar absorption spectra, etc.

The primary probes of dark perturbations can be broadly classified as either “light” or “matter”: The “light” probing the metric along trajectories which are close to null geodesics ( $ds^2 \simeq 0$ , e.g., CMB photons); the “matter” moving almost with the Hubble flow with non-relativistic peculiar velocities ( $|dx/d\tau| \ll 1$ , e.g., galaxies or Ly- $\alpha$  clouds). These two classes of probes, considered in Secs. 3.1 and 3.2 respectively, provide information that is complimentary in several respects, discussed in details in subsequent sections.

Linear theory adequately describes the inhomogeneous dynamics during horizon entry, when physical quantities are perturbed by about 0.001%, and long after the entry. Then the signatures of the dark kinetics are encoded in the linear transfer functions [alternatively, in Green’s functions

(Magueijo 1992; Baccigalupi 1999; Baccigalupi & Perrotta 2000; Bashinsky & Bertschinger 2001, 2002)], which are the essential constituents of “dynamical” cosmological observables, such as power spectra, luminosity functions, etc. To be specific (though general within the linear regime), in this section we consider an individual perturbation mode with a comoving wavevector  $\mathbf{k}$ .

#### 3.1. CMB

After horizon entry until photon decoupling around hydrogen recombination, a perturbation mode in the photon-baryon plasma undergoes acoustic oscillations. All the memory of the gravitational impact at the mode’s entry is then retained only in its oscillation amplitude  $A(\mathbf{k})$  and its temporal phase shift  $\varphi(k)$ . These quantities map into the heights and phase of the acoustic peaks in the observable CMB angular power spectra  $C_\ell$ , with a rough  $\ell \leftrightarrow k$  correspondence  $\ell \sim k r_{\text{dec}}$ , where  $r_{\text{dec}}$  is the angular diameter distance to the CMB decoupling surface. [In the standard  $\Lambda$ CDM model  $r_{\text{dec}} = \tau(z_{\text{dec}} \sim 1100) \simeq 14 \text{ Gpc.}$ ]

Our goal is to establish how  $A(\mathbf{k})$  and  $\varphi(k)$  are affected by the gravitational impact of perturbations in various species. As noted in the introduction, this task involves a subtlety that without proper care can lead to erroneous conclusions. Although the notion of density or temperature perturbation is uniquely defined in the FRW geometry, ambiguities arise on large scales in the perturbed metric. We argued in Sec. 2 that this complication is uniquely resolved in linear theory, where switching off a microscopic effect of interest results in the same change of observables regardless of other local properties of the various species. We can then calculate the observables in the models with the effect “on” and “off” and identify the *signature of the effect* with the difference. Being interested in the kinetics of perturbations, we compare the models with identical background expansion  $H(z)$ . For the compared models, we assume identical initial conditions, i.e., identical dynamics during the inflationary epoch, when the superhorizon perturbations likely were generated.

We describe the perturbative evolution by a formalism detailed in Bashinsky (2006). Then the gravitational forcing of perturbations appears concurrent with the responsible local interactions and the above unambiguous causal relations are manifest. In this formalism the general-relativistic generalization of particle overdensity is  $d \equiv \delta n_{\text{coo}}/n_{\text{coo}}$ , a perturbation of particle number density per *coordinate* volume.

When the CMB is tightly coupled to electrons by Thomson scattering, its (coordinate) overdensity evolves as

$$\ddot{d}_\gamma + \left( \frac{R_b}{1+R_b} \mathcal{H} + 2\tau_d k^2 \right) \dot{d}_\gamma + c_s^2 k^2 (d_\gamma - D) = 0 \quad (2)$$

(Bashinsky & Seljak 2004). Here and below  $R_b \equiv 3\rho_b/(4\rho_\gamma)$ , the diffusion time  $\tau_d = [1 - \frac{14}{15}(1+R_b)^{-1} + (1+R_b)^{-2}]/(6n_e\sigma_{\text{Thomp}})$  (Kaiser 1983) determines the Silk damping (Silk 1968), and  $c_s^2 = [3(1+R_b)]^{-1}$  gives the sound speed in the photon-baryon plasma. Only scalar perturbations are considered.<sup>4</sup> The gravitational driving of the CMB modes in eq. (2) is mediated through an instantaneous equilibrium value  $D$  of photon overdensity. In the Newtonian gauge (Mukhanov et al. 1992;

<sup>4</sup> The connection between dark dynamics and its observable signatures is relatively straightforward in the tensor sector, where gauge ambiguities are absent (Bardeen 1980; Kodama & Sasaki 1984). Vector perturbations, even if primordially generated, are not expected to survive superhorizon evolution (Bardeen 1980; Kodama & Sasaki 1984). If necessary, they can be analyzed similarly to the scalar perturbations.

Ma & Bertschinger 1995)

$$ds^2 = a^2 [-(1+2\Phi)d\tau^2 + (1-2\Psi)dx^2], \quad (3)$$

the driving term equals

$$D(\tau, k) = -3(\Phi + \Psi + R_b\Phi). \quad (4)$$

In the radiation era, when  $R_b \ll 1$ , the driving of the CMB by dark perturbations *on all scales* is controlled only by the sum  $\Phi + \Psi$ . This also applies to the CMB photons on all scales after their decoupling from baryons, c.f. the equation for the evolution of CMB intensity (5). Durrer (1994) argued that this is natural for the relativistic particles, whose dynamics is conformally invariant, and therefore should be sensitive only to the Weyl part of the curvature tensor. Indeed, the scalar part the Weyl tensor is fully specified by  $\Phi + \Psi$  (Durrer 1994). In the decoupled case, the driving by  $\Phi + \Psi$  is well known as the integrated Sachs-Wolfe effect (ISW) (R. K. Sachs, A. M. Wolfe 1967).

The full linear dynamics of partially polarized CMB photons and baryons (e.g., Ma & Bertschinger 1995) is also straightforward to formulate so that the changes of the apparent inhomogeneities are concurrent with the responsible local dark properties (Bashinsky 2006). In particular, the perturbation of the polarization-summed CMB intensity corresponds to its canonical variable  $\iota(x^\mu, n_i) \equiv I_\gamma/\bar{I}_\gamma - 1$  that evolves according to a transport equation (Durrer 1990; Bashinsky 2005, also presenting a fully nonlinear treatment)

$$\dot{\iota} + n_i \nabla_i \iota = -4n_i \nabla_i (\Phi + \Psi) + C_T, \quad (5)$$

where  $C_T$  is the Thompson collision term.

### 3.2. Matter

The evolution of linear scalar perturbations of cold dark matter (CDM) on all scales and, after decoupling from the CMB, of baryons on large scales is governed by the conservation and Euler equations

$$\dot{d}_c + \partial_i v_c^i = 0, \quad v_c^i + \mathcal{H}v_c^i = -\partial_i \Phi. \quad (6)$$

Their solution for a Fourier mode with non-singular (inflationary) initial conditions is

$$d_c = d_{c,\text{in}} - k^2 \int_0^\tau u_c d\tau, \quad u_c = \frac{1}{a} \int_0^\tau (a\Phi) d\tau. \quad (7)$$

The quantity  $u_c$  that appears in these equations is physically the CDM velocity potential:  $v_c^i = -\partial_i u_c$ .

Similarly to the CMB modes, the matter perturbations carry the memory of the metric inhomogeneities at the horizon entry in two independent functions: the *overdensity change* and *velocity boost* that were generated during the entry. After horizon entry, the excess of CDM velocity, decaying as  $1/a$ , yet not vanishing instantaneously, continues to enhance matter clumping. Hence, the implications of the velocity boost for the observed  $\delta\rho_m/\rho_m$  are generally more important than the initial overdensity enhancement (Hu & Sugiyama 1996).

Eqs. (7) show that matter perturbations are driven by the potential  $\Phi$  alone *on all scales* (Bashinsky & Seljak 2004). This also has a natural explanation. In the Newtonian gauge, the point particles of a mass  $m$  are described by the Lagrangian  $L = -m\sqrt{-ds^2}/d\tau = -ma\sqrt{[1+2\Phi(\mathbf{x})] - [1-2\Psi(\mathbf{x})]\dot{\mathbf{x}}^2}$ . The corresponding contribution of  $\Psi$  is negligible for nonrelativistic particles, when  $L \simeq ma[\dot{\mathbf{x}}^2/2 - \Phi(\mathbf{x})] + \text{const}$ . Moreover, the initial (superhorizon) perturbations of particle's coordinates  $\mathbf{x}$  determine the initial value of the *coordinate* overdensity  $d_c$  also independently of  $\Psi$ .

Since the CMB, on the other hand, is affected by the sum  $\Phi + \Psi$ , this is one of the respects in which matter and the CMB provide complimentary information about dark inhomogeneities. A combined analysis of both probes is particularly useful for testing a deviation of  $\Psi/\Phi$  from unity, produced by freely streaming species (e.g., Ma & Bertschinger 1995) or generally expected in modified gravity (Bertschinger 2006; Dodelson & Liguori 2006).

## 4. PARAMETERIZING DARK DYNAMICS

In this section we review several general parameterizations of the potentially observable properties of the dark universe. We start from the spacetime metric, connected most directly to observational probes. Then, assuming validity of the Einstein equations, we match the metric characteristics to a general description of dark densities and stresses. Finally, we consider a parameterization of the potentially measurable properties of dark internal dynamics. The observational probes of these parameters will be studied in Sec. 5. The status of these parameterizations in cosmologies with modified gravity will be addressed in Sec. 6.

### 4.1. Metric

Provided the visible matter couples covariantly and minimally to a certain metric tensor  $g_{\mu\nu}$ , the observable impact of dark sectors or modified gravity alike can be parameterized by a single function of redshift  $z$ , to describe the FRW background, and by two independent functions of  $z$  and  $\mathbf{k}$ , to specify scalar metric perturbations. For example, the background can be quantified by its expansion rate  $\mathcal{H}(z)$  (with its possible spatial curvature), and the metric perturbations by the Newtonian-gauge potentials  $\Phi(z, \mathbf{k})$  and  $\Psi(z, \mathbf{k})$ .

### 4.2. Densities and stresses

For a more direct link to the internal properties of the dark sectors, it may be worthwhile to parameterize their contribution to the energy-momentum tensor  $T^{\mu\nu} = \sum_a T_a^{\mu\nu}$ . If gravity is described by general relativity then  $T^{\mu\nu}$  determines the geometrical quantities  $\{\mathcal{H}, \Phi, \Psi\}$  through the Einstein equations. In this view, the background may be specified by the average energy densities of the species  $\rho_a(z) \equiv -T_{0(a)}$ . The scalar inhomogeneities of the metric are determined from the perturbations of the energy densities, sourcing the curvature potential  $\Psi$ , and from anisotropic stress, generating the splitting  $\Phi - \Psi$ . The corresponding formulas are given next.

After Hu (1998), we will use proper particle number overdensity  $\delta_a^{(c)}(z, \mathbf{k}) \equiv \delta\rho_a^{(c)}/(\rho_a + p_a)$  in the *comoving* gauge<sup>5</sup>. In any other gauge

$$\delta_a^{(c)} = \frac{\delta\rho_a}{\rho_a + p_a} + 3\mathcal{H}u_a, \quad (8)$$

where  $v_a^i = -\partial_i u_a$ . Specifically,  $\delta_a^{(c)}$  can be expressed in terms of the dynamical coordinate overdensities  $d_a$ , used in Sec. 3, as

$$\delta_a^{(c)} = d_a + 3\mathcal{H}u_a + 3\Psi. \quad (9)$$

The comoving-gauge overdensity  $\delta_a^{(c)}$  is convenient for two reasons. First, it directly sources the Newtonian potential  $\Psi$  (Bardeen 1980)

$$\nabla^2 \Psi = 4\pi G a^2 \sum_a (\rho_a + p_a) \delta_a^{(c)}, \quad (10)$$

<sup>5</sup> The comoving gauge conditions for scalar perturbations are zero total momentum density ( $T_i^0 \equiv 0$ ) and vanishing shear of the spatial metric ( $g_{ij} \propto \delta_{ij}$ ).

where  $\nabla^2 \equiv ({}^3\bar{g}^{ij}\partial_i\partial_j)$  is the spatial Laplacian (from now on the background is assumed flat). Second, the generalized pressure gradient in the Euler equation [the term  $-\partial_i f_p$  in eq. (19)] in the comoving gauge takes its usual special-relativistic form [ $f_p = \delta p^{(c)}/(\rho+p)$ ].

Nevertheless, we view  $\delta_a^{(c)}$  only as a useful linear combination (9), rather than an independent dynamical variable: The evolution of  $\delta_a^{(c)}$ , unlike that of  $d_a$ , is highly nonlocal. Beyond the horizon  $\delta_a^{(c)}$ , unlike the frozen  $d_a$ , is affected by all species, in addition to the studied dark species  $a$ . In terms of the dynamical variables  $d_a$  and  $u_a$  the Poisson equation (10) reads

$$\left(-3 + \frac{\nabla^2}{\gamma}\right)\Psi = \sum_a x_a (d_a + 3\mathcal{H}u_a), \quad (11)$$

with

$$\gamma \equiv 4\pi G a^2 (\rho + p) = \frac{3}{2}(1+w)\mathcal{H}^2, \quad \text{and} \quad x_a \equiv \frac{\rho_a + p_a}{\rho + p}. \quad (12)$$

Unlike eq. (10), the generalized Poisson equation in the form (11) in the superhorizon limit is explicitly non-singular and its solution  $\Psi \approx -\frac{1}{3}(d + 3\mathcal{H}u)$  even becomes local.

We describe the scalar component of the anisotropic stress  $\Sigma_j^i \equiv T_j^i - \frac{1}{3}\delta_j^i T_k^k$  by a potential  $\sigma(z, \mathbf{k})$  as

$$(\partial_i\partial_j - \frac{1}{3}\delta_j^i\nabla^2)\sigma_a \equiv \frac{\Sigma_{j(a)}^i}{(\rho_a + p_a)}. \quad (13)$$

The corresponding gravitational equation is (Bardeen 1980; Kodama & Sasaki 1984; Ma & Bertschinger 1995):

$$\Phi = \Psi - 8\pi G a^2 \sum_a (\rho_a + p_a)\sigma_a. \quad (14)$$

Thus the densities and stresses of the background and scalar perturbations may be parameterized by a set  $\{\rho_a(z), \delta_a^{(c)}(z, \mathbf{k}), \sigma_a(z, \mathbf{k})\}$  for each sector  $a$ . Both  $\delta_a^{(c)}$  and  $\sigma_a$ , as defined by eqs. (8) and (13), are gauge-invariant quantities. Neither of them, though, can be measured locally.

#### 4.3. Dynamical properties

As a step further, we can try to parameterize the *dynamics* of the dark densities and stresses. One such useful and popular parameterization has been suggested by Hu (1998). He described the dynamics of the background by the conventional ‘‘equation of state’’  $w_a(z) \equiv p_a/\rho_a$ , and the dynamics of perturbations by the effective sound speed

$$c_{\text{eff},a}^2(z, k) \equiv \delta p_a^{(c)}(k)/\delta \rho_a^{(c)}(k). \quad (15)$$

We call this quantity ‘‘stiffness’’ throughout the paper in order to distinguish it from the physical velocity of perturbation propagation  $c_p$ , Sec. 5.3, which may differ from  $c_{\text{eff}}$  and is probed by different observables.

In addition, Hu (1998) considered a ‘‘viscosity parameter’’  $c_{\text{vis},a}^2(z, k)$  (defined by the ratio of the dynamical change of anisotropic stress to the velocity gradient). However, realistically the evolution of anisotropic stress is determined not only by the velocity gradient but also by additional degrees of freedom, e.g., by the  $\ell = 3$  multipole or polarization. Therefore, in our study we will not use  $c_{\text{vis}}^2$  but will work directly with  $\sigma_a(z, k)$ .

A dark sector that couples negligibly to the other species can be assigned a covariantly conserved energy-momentum tensor  $T_{(a)}^{\mu\nu}$  through the standard procedure of metric variation (e.g., Landau & Lifshitz 1975). Given the value of the sector’s background energy density  $\rho_a$  at some moment (e.g. the present

density, set by  $\Omega_a h^2$ ),  $w_a(z)$  determines the density at all times from

$$\dot{\rho} = -3\mathcal{H}(1+w)\rho \quad (16)$$

(the subscript  $a$  is dropped from now on.) The evolution of density perturbation  $d$  follows by linearly perturbing the equation of energy conservation  $T^{0\nu}{}_{;\nu} = 0$ :

$$\dot{d} + \partial_i v^i = Q \quad (17)$$

with<sup>6</sup>

$$Q \equiv \frac{\dot{\rho}\delta p - \dot{p}\delta\rho}{(\rho+p)^2} = -3\mathcal{H}\left(c_{\text{eff}}^2 - \frac{\dot{p}}{\rho}\right)\delta^{(c)}. \quad (18)$$

Linearization of  $T^{i\nu}{}_{;\nu} = 0$  yields the evolution of momentum-averaged velocity:<sup>7</sup>

$$\dot{v}^i + \mathcal{H}v^i = -\partial_i\Phi - \partial_i f_p + F_\sigma^i \quad (19)$$

with

$$f_p \equiv \frac{\delta p - \dot{p}u}{\rho + p} = c_{\text{eff}}^2 \delta^{(c)}, \quad (20)$$

$$F_\sigma^i \equiv -\frac{\partial_j \Sigma^{ij}}{\rho + p} = \frac{2}{3}\partial_i \nabla^2 \sigma. \quad (21)$$

We remember that  $\delta^{(c)}$  is given by eq. (9), and the gravitational potentials are determined by the linearized Einstein equations (10) and (14). These equations are closed after  $c_{\text{eff}}^2$  and  $\sigma$  are specified by the species’ internal dynamics. The expansion of perturbations over Fourier modes splits the equations into uncoupled systems for each mode, with its own  $c_{\text{eff}}^2(k)$  and  $\sigma(k)$ .

Similarly to  $\sigma(k)$ , the stiffness  $c_{\text{eff}}^2(k)$  is manifestly gauge-invariant but not measurable locally.

#### 4.4. Other parameterizations

Any of the above sets  $\{\mathcal{H}, \Phi, \Psi\}$ ,  $\{\rho, \delta^{(c)}, \sigma\}$ , or  $\{w, c_{\text{eff}}^2, \sigma\}$  parameterizes all properties of arbitrary dark sectors that can be constrained by any probe of background and scalar perturbations. It may nevertheless be useful to explore other internal properties of the dark species. Certain properties, e.g. particle masses and cross-sections, that are not readily extractable from the above sets may be important for particle-physics models. Other properties may have more distinctive or less degenerate observable signatures. An example appears in Sec. 5.3, discussing the dark characteristics that control the additive shift of the CMB peaks.

Of course, yet alternative parameterizations of the internal dark dynamics may also be considered. For example, Linder (2005) suggested to approximately quantify the growth of cosmic structure by a growth index parameter  $\gamma$ . This approach may be useful for utilizing LSS to probe modified gravity or non-standard long-range interaction. We do not pursue it here, being interested in more universal descriptions that are applicable to the CMB as well.

### 5. MAPPING DARK DYNAMICS TO OBSERVABLE FEATURES

In this, main, section we identify the observable signatures of the dark properties. Specifically, we consider the signatures of: anisotropic stress, the dark species’ stiffness, the propagation speed of their inhomogeneities, and their clustering. The observational probes considered are the transfer functions for cosmic structure and the power spectra of the CMB.

<sup>6</sup>  $\dot{p}/\rho$ , appearing in eq. (18), can be related to the background equation of state  $w$  as  $\dot{p}/\rho = w - \frac{\dot{w}}{3(1+w)\mathcal{H}}$ .

<sup>7</sup> Eqs. (19)–(21) are simpler in terms of the velocity potential: for  $v^i = -\partial_i u$ , they read

$$\dot{u} + \mathcal{H}u = \Phi + c_{\text{eff}}^2 \delta^{(c)} - \frac{2}{3}\nabla^2 \sigma.$$

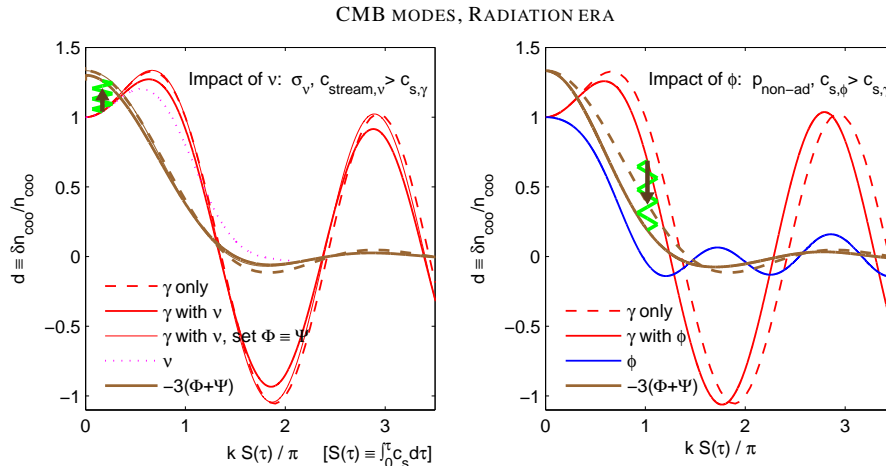


FIG. 1.— The evolution of CMB overdensity  $d_\gamma(\tau, k)$  (oscillating, red curves) and the corresponding gravitational driving term  $D = -3(\Phi + \Psi)$  (monotonically falling, brown curves) in the radiation era for  $R_b \ll 1$  and negligible photon diffusion. The gravitational driving of the CMB [eq. (2)] is illustrated with a spring that connects the  $d_\gamma$  and  $D$  curves. The panels demonstrate the impact of perturbations in decoupled neutrinos (left) and quintessence (right). —Left panel shows  $d_\gamma$  and  $D$  for: tightly-coupled photons only (dashed), the standard model with three neutrinos (wider solid), and the same model after switching off neutrino anisotropic stress as a source of  $\Phi - \Psi$  (thinner solid). —Right panel displays: the earlier photon-only model (dashed) and a fictitious model where, as in the standard model, 59% of energy density is in photons but the remaining 41% is now in a tracking quintessence  $\phi$ , with  $w_\phi = 1/3$  (solid).

### 5.1. Anisotropic stress

Already in the standard cosmological model, significant anisotropic stress is generated in the radiation era by freely streaming neutrinos. The anisotropic stress in our universe may differ from the standard three-neutrino expectation because of, for example, additional free-streaming relativistic species, which would enhance the stress. Or, it may differ because of non-minimal neutrino couplings (Chacko et al. 2004, 2005; Beacom et al. 2004; Okui 2005; Hannestad 2005; Grossman et al. 2005), which would locally isotropize neutrino velocities and reduce or eliminate their anisotropic stress. Anisotropic stress  $\sigma$  changes  $\Phi$  and  $\Psi$  (Ma & Bertschinger 1995) and consequently the CMB gravitational driving term  $D$  (4) even on superhorizon scales. Thus the  $\sigma$  of dark species affects the CMB modes since the earliest stages of horizon entry.

The left panel of Fig. 1 shows the evolution of gravitationally coupled photon and neutrino perturbations in the radiation era for various assumptions about neutrino abundance and properties. The plots are obtained by numerically integrating the corresponding equations from Bashinsky (2006). The oscillating, red curves give the CMB overdensity  $d_\gamma(\tau, k)$ . The falling, brown curves show the driving term  $D(\tau, k)$ , equal to  $-3(\Phi + \Psi)$  in the radiation era.

As evident from this figure, the photon overdensity  $d_\gamma$  in the presence of freely streaming neutrinos (wider solid oscillating curve) is suppressed with respect to  $d_\gamma$  of a neutrinoless model (dashed oscillating curve). The suppression of the CMB perturbations by neutrinos can be related to the reduction of  $D$  early during horizon entry, with the CMB modes then experiencing a smaller initial boost.

The suppression of  $D$  and, consequently, of the CMB oscillations in the Newtonian gauge is due to  $\sigma_\nu$  being a direct source of gravitational potentials. It is not due to the damping of neutrino perturbations by the viscosity effect of  $\sigma_\nu$ , eqs. (19) and (21). We can verify this by repeating the calculations for the standard model with three neutrinos but with the following modification: We remove the gravitational effect of anisotropic stress in eq. (14), i.e., set  $\Phi = \Psi$ . We make no other changes in

the integrated equations, i.e., preserve the Poisson equation (10) and use the standard dynamical equations for all species' perturbations. In particular, we retain the  $\sigma_\nu$  viscosity term in the  $\dot{v}_\nu$  equation [c.f. eqs. (19, 21)]. The results of this calculation, with the “gravity of  $\sigma_\nu$  removed”<sup>8</sup>, are plotted on the left panel of Fig. 1 with the thinner solid curves. Switching off the direct gravitational effect of  $\sigma_\nu$  is seen to lift the neutrino suppression of the subhorizon CMB oscillations.

On the scales that enter the horizon in the radiation era ( $\ell \gg 200$ ) the suppression of the amplitude of the CMB oscillations,  $A_\gamma$ , can be calculated analytically in leading order in  $R_\nu \equiv \rho_\nu / (\rho_\gamma + \rho_\nu)$  (Bashinsky & Seljak 2004). For all physical values  $0 \leq R_\nu \leq 1$ , this suppression is well fitted by (Hu & Sugiyama 1996)

$$\frac{A_\gamma}{A_\gamma(R_\nu \rightarrow 0)} \approx \left(1 + \frac{4}{15} R_\nu\right)^{-1}, \quad (22)$$

where  $R_\nu$  is varied at unchanged fluctuations of the primordial curvature  $\zeta$  (Bardeen et al. 1983). This variation implies fixed inflationary physics, although then the superhorizon values of both  $\Phi$  and  $\Psi$  change with  $R_\nu$ . The oscillations in the CMB power spectra of temperature, polarization, or their cross-correlation for  $\ell \gg 200$  are suppressed by the square of (22).

To summarize, the suppression of the CMB oscillations by freely streaming neutrinos is due to neutrino anisotropic stress. In the Newtonian gauge the suppression may be attributed to the anisotropic stress acting as a source of metric perturbations, impacting CMB photons. The damping of bulk velocity and density perturbations of neutrinos by streaming plays almost no role in the suppression of CMB fluctuations.

<sup>8</sup> The performed removal of  $\sigma_\nu$  from the gravitational equation (14) but not from the Euler equation (19) violates the covariance of the Einstein equations. Therefore, the separation of the effects of anisotropic stress into “gravitational” and “dynamical” should not be considered beyond the context of the Newtonian gauge. We could preserve the Einstein equations by removing  $\sigma_\nu$  from both eqs. (14) and (19). The result would be the neutrinoless model, described on the left panel of Fig. 1 by the dashed curves; again, showing no suppression of the CMB amplitude.

### 5.2. Stiffness $c_{\text{eff}}^2$

The quantity  $c_{\text{eff}}^2(z, k) \equiv \delta p^{(c)}/\delta \rho^{(c)}$  describes the stiffness of the dark medium to perturbations with a wavevector  $k$ . (We avoid calling  $c_{\text{eff}}^2$  “the sound speed,” not to mix it with  $c_p$  of Sec. 5.3.) The stiffness  $c_{\text{eff}}^2$  affects directly the evolution of the dark species’ overdensities and peculiar velocities. The direct impact of  $c_{\text{eff}}^2$  on the evolution of overdensity, eq. (17), is described by the term  $Q$  (18), proportional to the so called “non-adiabatic” pressure  $\delta p - (\dot{p}/\dot{\rho})\delta\rho$ . The velocities are accelerated by pressure gradient, the term  $-\partial_i f_p = -\partial_i(c_{\text{eff}}^2 \delta \rho_a^{(c)})$  in eq. (19), directly proportional to  $c_{\text{eff}}^2$ . For perfect fluids and  $k \gg \mathcal{H}$ , the quantity  $c_{\text{eff}}^2(k)$  gives the (phase) velocity of acoustic waves. In general, however,  $c_{\text{eff}}^2$  need not be related to the speed of perturbation propagation, which will be studied in Sec. 5.3.

The dependence of the dark perturbations’ evolution on their stiffness  $c_{\text{eff}}^2$  is reflected in the perturbations’ contribution to metric inhomogeneities. Through the latter, the dark stiffness affects the visible species (e.g., Erickson et al. 2002). To be specific, we assume that superhorizon perturbations are adiabatic.<sup>9</sup> Then the comoving overdensity  $\delta^{(c)}$ , eq. (8), vanishes in the superhorizon limit. Consequently,  $\dot{d}_a$  [eqs. (17-18)] and  $\dot{v}_a$  [eqs. (19-20)] depend on  $c_{\text{eff}}^2$  only at the order  $O(k^2\tau^2)$ . The sourced potentials  $\Psi$  and  $\Phi$  therefore become sensitive to  $c_{\text{eff}}^2$  only at a late period of the horizon entry, also only at the order  $O(k^2\tau^2)$ . Note that, as discussed in Sec. 5.1, anisotropic stress, in contrast, changes the potentials even in the superhorizon limit  $k\tau \rightarrow 0$ . Thus  $c_{\text{eff}}^2$  affects the observable species at a noticeably *later* stage of the horizon entry than  $\sigma$  does.

The lateness of the impact of  $c_{\text{eff}}^2$  is clearly seen on the right panel of Fig. 1, which shows the joint evolution of perturbations in a photon fluid and a classical scalar field  $\phi$  (quintessence). The quintessence background density is set to track radiation ( $w_\phi = 1/3$ ) but its stiffness exceeds that of the photon fluid ( $c_{\text{eff},\phi}^2 = 1 > c_{\text{eff},\gamma}^2 = 1/3$ , e.g., Hu (1998)). Either the perturbations of the quintessence (right panel) or of freely streaming neutrinos (left panel and previous Sec. 5.1) decrease the CMB-driving sum  $\Phi + \Psi$ . With neutrinos,  $\Phi + \Psi$  was decreased already on superhorizon scales by neutrino anisotropic stress ( $\sigma_\nu \neq 0 = \sigma_{\gamma b}$ ). On the other hand, in agreement with the previous arguments,  $\Phi + \Psi$  is seen to be affected by the stiff inhomogeneities of quintessence, whose anisotropic stress is zero, at a later time.

There are several observable consequences of the lateness of the influence of dark stiffness on potentials. First, while the early reduction of  $\Phi + \Psi$  by  $\sigma_\nu$  suppressed the amplitude of the acoustic oscillations in  $d_\gamma$ , the later reduction of  $\Phi + \Psi$  by large  $c_{\text{eff},\phi}^2$  slightly *enhances* this amplitude. The right panel of Fig. 1 explains this paradox: The reduction of  $\Phi + \Psi$  by quintessence perturbations increases the negative driving of photon overdensity when  $\dot{d}_\gamma$  is on average negative. As a result, the acoustic oscillations gain energy and their amplitude increases.

The lateness of the stiffness impact has another important consequence. Namely, the ratio of the matter response over the CMB response is considerably larger to probing  $c_{\text{eff}}^2$  than to probing  $\sigma$ . This is evident from comparing the left panel of Fig. 2, showing CDM overdensity (black, rising curves), and the earlier Fig. 1, for the CMB overdensity, all in the radi-

ation era. In Fig. 2, CDM overdensity  $d_c$  is plotted for: the photon-only model, where  $\sigma = 0$  (dashed); the standard model with 59% of energy density in coupled photons and 41% in streaming neutrinos (wide solid); and a fictitious model with the same 59% of energy density in photons but the remaining 41% carried by quintessence (thin solid). We see that the enhanced stiffness of the dark component of the third model impacts the matter an order of magnitude more strongly than the anisotropic stress of the second model. On the other hand, the CMB perturbations, studied on the left and right panels of Fig. 1, are affected by neutrinos and quintessence of the second and third models comparably.

These results have a simple explanation. The early impact of  $\sigma$  on matter velocities is washed out over time by the Hubble friction [ $\mathcal{H}v_c^i$  term in eq. (6)]. The Hubble friction, acting on massive CDM and baryons, damps less the  $c_{\text{eff}}^2$ -dependent late impact of dark perturbations on matter. The overdensity of relativistic photons, on the other hand, is unchanged by Hubble friction [see eq. (2), where  $R_b$  is negligible]. Hence the present CMB anisotropy responds comparably to either of the impacts.

The relatively high ratio of the matter over the CMB responses to the dark stiffness should help distinguish an excess of relic relativistic particles in the radiation era from a subdominant tracking quintessence. Both the decoupled relativistic relics and quintessence have a similar nondegenerate phase-shift signature in the CMB power spectra (Bashinsky & Seljak 2004, more in Sec. 5.3 below). This signature will soon considerably tighten the constraints on neutrinos or an early quintessence with the enhanced angular resolution of CMB experiments. Yet it does not discriminate between the two scenarios if a nonstandard signal is observed. The discrimination can, however, be achieved by combining the CMB data with accurate measurements of matter power, together sensitive to the strong effect of quintessence on the ratio of the CMB and matter power. The discrimination should be facilitated by the fact that tracking quintessence and an excess of relativistic species change this ratio in opposite directions.

### 5.3. The speed of sound or streaming

Dark inhomogeneities were seen to affect the amplitude of the oscillations in the CMB temperature and polarization power spectra. In addition to the heights of the acoustic peaks, the CMB spectra are characterized by the peaks’ positions  $\ell_n$ . The period,  $\ell_A$ , of the acoustic oscillations is well known to be controlled entirely by background geometry and the properties of the photon-baryon plasma. (Namely,  $\ell_A = \pi r_{\text{dec}}/S_{\text{dec}}$ , where  $r_{\text{dec}}$  is the distance to the surface of CMB decoupling and  $S_{\text{dec}} = \int_0^{\tau_{\text{dec}}} c_{\gamma b} d\tau$  is the corresponding size of the acoustic horizon.) On the other hand, the overall additive shift of the peak’s sequence, i.e., the parameter  $\Delta\ell$  in an approximate relation  $\ell_n \sim n\ell_A + \Delta\ell$  is a robust characteristic of dark perturbations.<sup>10</sup>

The shift of the peaks in  $\ell$  is determined by the shift  $\Delta\varphi$  of the temporal phase of the subhorizon modes,  $d_\gamma = A_\gamma \cos(kc_{\gamma b}\tau - \Delta\varphi)$ , as  $\Delta\ell = \ell_A \Delta\varphi/\pi$ . This shift of phase is tightly connected to the locality of the inhomogeneous dynamics (Bashinsky & Seljak 2004; Bashinsky 2004). This becomes manifest in the real-space description of perturbation evolution of Bashinsky & Bertschinger (2001, 2002), using plane-

<sup>9</sup> The following arguments remain valid under a considerably milder condition: It is sufficient that the primordial perturbations in the probed dark species are *internally* adiabatic (Bashinsky & Seljak 2004). In particular, this condition is satisfied automatically for any one-component fluid.

<sup>10</sup> The positions of individual peaks receive additional corrections from the changes of the peaks’ shape, such as due to the Silk damping and (for temperature) falling Doppler contribution. These corrections are fixed by the background properties and should not spoil the constraints on the overall shift  $\Delta\ell$ .

parallel Green's functions. The Green's function of  $d_\gamma$  in the radiation era, when the modes forming the acoustic peaks enter the horizon, was found in Bashinsky & Seljak (2004). Its Fourier transform yields

$$\Delta\varphi \simeq -\pi\sqrt{3}(\Phi + \Psi)_{|x|=c_s\tau} \quad (23)$$

(for  $|\Delta\varphi| \ll 1$ .) Here, the initial conditions are assumed adiabatic, and  $c_s \equiv c_{\gamma b} = 1/\sqrt{3}$  is the speed of sound in the radiation era. The term  $(\Phi + \Psi)_{|x|=c_s\tau}$  is the value of  $\Phi + \Psi$  at the acoustic horizon of a perturbation that is initially localized in space to a thin plane:  $d(\tau \rightarrow 0, x) = \delta_D(x)$ , where  $\delta_D(x)$  is the Dirac delta function. For adiabatic initial conditions,  $(\Phi + \Psi)_{|x|=c_s\tau}$  is fully determined by the perturbations that propagate beyond the acoustic horizon. In particular,  $(\Phi + \Psi)_{|x|=c_s\tau} = 0$  if none of the dark species support perturbations that propagate faster than the acoustic speed  $c_s$ . [For a proof, accounting for subtleties of inhomogeneous gravitational dynamics on large scales, see Appendix B of Bashinsky & Seljak (2004).]

Two commonly considered types of cosmological species do support perturbations that propagate faster than  $c_s$ . These are decoupled relativistic neutrinos and quintessence, in both of which perturbations propagate at the speed of light. The increase of the energy density in either of these species by one effective fermionic degree of freedom displaces the peaks of the CMB temperature and E-polarization spectra by  $\Delta l_{+1\nu} \simeq -3.4$  for neutrinos (Bashinsky & Seljak 2004) and  $\Delta l_{+1\varphi} \simeq -11$  for tracking quintessence (Bashinsky 2006). This nondegenerate effect will lead to tight constraints on the abundance (Lopez et al. 1999; Bowen et al. 2002; Bashinsky & Seljak 2004; Perotto et al. 2006) and interaction (Chacko et al. 2004) of the relic neutrinos from upcoming CMB experiments. These constraints notably improve with higher angular resolution in temperature and polarization as new data at higher  $\ell$ 's allow better identification of the oscillations' phase. [The polarization channel, where the acoustic peaks are more pronounced, is especially useful (Bashinsky & Seljak 2004).]

Thus a crucial characteristic that affects the acoustic phase is the velocity  $c_p$  of the wavefront of a localized perturbation of dark species, shifting the phase if and only if  $c_p > c_s \approx 1/\sqrt{3}$ . The velocity  $c_p$  of a perfect fluid or a classical field is determined by the stiffness  $c_{\text{eff}}^2$ . However, in general  $c_p$  and  $c_{\text{eff}}$  are independent. As a notable example, free-streaming relativistic particles have  $c_{\text{eff}}(k) \equiv 1/\sqrt{3}$  but  $c_p = 1$ . Unlike  $c_{\text{eff}}(k)$ ,  $c_p$  is defined irrespectively of any gauge and is locally measurable. Finally, as discussed in Sec. 5.2 and the present section, the quantities  $c_{\text{eff}}$  and  $c_p$  map to different observable signatures. Thus for gaining robust knowledge of the nature and kinetics of dark radiation, including neutrinos and possible early quintessence, it is important to constrain observationally both  $c_{\text{eff}}(k)$  and  $c_p$ .

#### 5.4. $\Phi$ and $\Psi$ ; clustering in the dark sectors

In the three previous subsections we analyzed the gravity-mediated signatures of the dark stresses. Now we shift our attention to the observational manifestations of potentials  $\Phi$  and  $\Psi$  themselves, irrespectively of their cause or even of the validity of the Einstein equations. As described quantitatively in this subsection, the impact of the gravitational potentials on large-scale structure (LSS) and the CMB differs in several essential ways. Consequently, the corresponding constraints will be rather complimentary.

Before considering the observable impact of the metric potentials, let us summarize the scenarios in which the potentials

are expected to differ from the predictions of the standard cosmological model. As compared to a typical model with CDM and quintessence dark energy (including  $\Lambda$ CDM model as a limiting case), different  $\Phi$  and  $\Psi$  in a given background  $w(z)$  are expected:

- During horizon entry for practically any other dark energy model.
- On any scales for models with modified gravity.
- On subhorizon scales for models with non-canonical kinetic term for the field (Armendariz-Picon et al. 2001), models with warm dark matter (Blumenthal et al. 1982; Olive & Turner 1982) or with interacting dark matter (Carlson et al. 1992; de Laix et al. 1995; Spergel & Steinhardt 2000). More mundane physics affecting the subhorizon potentials includes thermal, radiative, or magnetic pressure on baryons, and various astrophysical feedback mechanisms (supernovae, central black holes, etc.)

##### 5.4.1. Matter response

Cosmic structure, which growth in the matter era is driven by potential  $\Phi$ , is very sensitive to modifications of  $\Phi$  by new physics at low redshifts. As noted in Sec. 5.2, the Hubble friction diminishes its sensitivity toward higher redshifts. The matter power spectrum and other characteristics of cosmic structure are therefore the natural probes of the scenarios in the above classes (b) and (c).

An example is shown on the right panel of Fig. 2. For both scenarios displayed on this panel the background is Einstein–de Sitter. The solid curves show the growing matter overdensity and gravitational potential in a pure CDM phase. [The plotted potential is weighted by  $\tau$  according to eq. (24).] The dashed curves display the same quantities for a toy scenario in which CDM constitutes only 50% of the energy density, while the other 50% is in a classical scalar field with  $w_\phi = w_{\text{CDM}} \equiv 0$ . Since for the field  $\delta p_\phi^{(c)}/\delta\rho_\phi^{(c)} = c_{\text{eff}}^2 = 1$ , its clustering is suppressed and its perturbations do not contribute to the subhorizon potential. Correspondingly, the structure growth in the second scenario is seen to be significantly suppressed. Note that both scenarios have identical background expansion and the standard laws of gravity.

Quantitatively, the impact of the potential  $\Phi$  over time ( $\tau, \tau + \Delta\tau$ ) on matter overdensity  $d_c$  observed at a later time  $\tau' \gg \tau$  scales roughly as  $(\tau\Delta\tau)\Phi$ . The prefactor  $\tau\Delta\tau$  quantifies the stronger suppression of an early impact by the higher Hubble friction, experienced by matter particles during the faster cosmological expansion. The derivation follows straightforwardly from eq. (7): A nonzero potential  $\Phi(\tau)$  over the time interval  $(\tau, \tau + \Delta\tau)$  contributes to the matter overdensity at a later time  $\tau'$  as<sup>11</sup>

$$\begin{aligned} \Delta\left(\frac{\delta\rho_c}{\rho_c}\right)_{\tau'} &= \Delta d_c(\tau') = -k^2 a(\tau)\Phi(\tau)\Delta\tau \int_\tau^{\tau'} \frac{d\tau''}{a(\tau'')} \\ &\sim -k^2\Phi(\tau)\tau\Delta\tau. \end{aligned} \quad (24)$$

In the models with standard gravity, CDM, and *insignificant clustering of dark energy*, the dark energy perturbations

<sup>11</sup> The last estimate in eq. (24) assumes that  $w \leq 1/3$ , so that  $a(\tau)$  grows as  $\tau$  or faster. The zero of conformal time  $\tau$  is chosen, as usual, as  $\tau \rightarrow 0$  when  $a \rightarrow 0$ . Logarithmic corrections that appear for  $w = 1/3$  (radiation domination) are ignored.

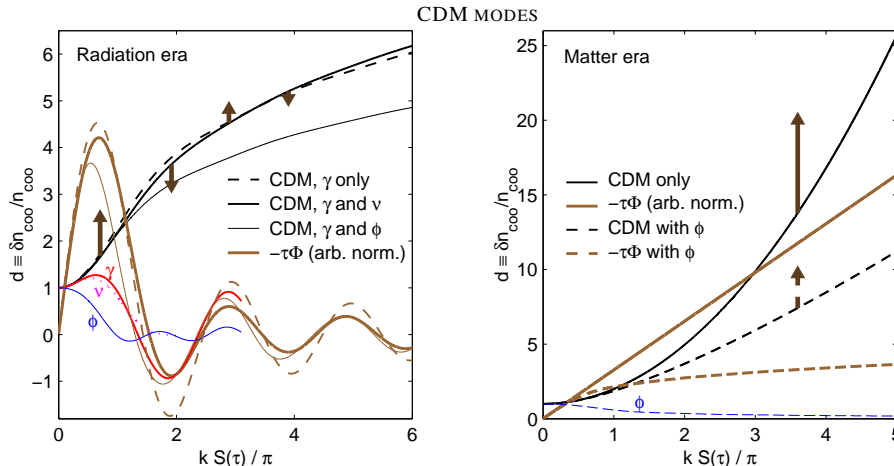


FIG. 2.— Growth of CDM overdensity  $d_c(\tau, k)$  (rising black) during radiation domination (left) and matter domination (right). Brown curves show the value of  $\tau\Phi$ , responsible for the ultimate growth of  $\delta\rho_c/\rho_c$  by a future time of its observation, eq. (24). — Left: coupled photons only (dashed), photons plus 3 standard neutrinos (wide solid), and photons plus a tracking ( $w_\phi = 1/3$ ) scalar field  $\phi$  replacing the neutrino density of the previous model (thin solid). — Right: pressureless matter only (solid), and a model with equal densities of matter and a scalar field that tracks it,  $w_\phi = 0$  (dashed).

can leave their mark on the potential only during horizon entry. By eq. (24), the corresponding early potential contributes to structure growth much less than the potential generated long after the entry by the clustered CDM and baryons. Thus in the absence of the non-standard physics of the types (b) or (c) above, it is justified to consider an approximate consistency relation between the background equation of state  $w(z)$  and the growth of cosmic structure (Knox et al. 2005; Ishak et al. 2006; Chiba & Takahashi 2007).

As we see next, the situation is essentially *opposite* when the dark sectors are probed by the primary anisotropies of the CMB.

#### 5.4.2. CMB response

Metric perturbations have a dramatic impact on CMB temperature anisotropies. In sharp contrast to large scale structure, primary CMB anisotropies (generated by linear evolution) depend most strongly on the values and evolution of gravitational potentials *during horizon entry*. They are only mildly sensitive to the potentials on subhorizon scales. (This need not to apply to secondary anisotropies.)

The scalar perturbations of the CMB respond primarily to the sum of the Newtonian-gauge potentials  $\Phi + \Psi$  on all scales and all times (Sec. 3.1). While the inertial drag of the CMB by baryons, affected by  $\Phi$  alone, is important for the CMB sensitivity to the baryon density and is noticeable around decoupling (Hu & Sugiyama 1996), it never dominates the evolution of CMB perturbations. For developing a general understanding of the CMB sensitivity to dark dynamics we will often ignore it.

We stressed in Sec. 2 that dark inhomogeneities at a (conformal) time  $\tau$  and the metric perturbations generated by them affect only the modes with  $k \gtrsim \mathcal{H} \sim 1/\tau$ . The corresponding dynamics of CMB perturbations differs qualitatively in a tightly coupled regime, prior to hydrogen recombination at  $z_{\text{rec}} \sim 1100$ , and in a streaming regime, after recombination. We will consider the CMB response to the metric perturbation  $\Phi + \Psi$  at these two epochs in turns. In the subsequent Sec. 5.4.3 we will quantify this response by simple analytical formulas. We will see that despite numerous differences in the evolution of CMB modes before and after recombination, the CMB response to

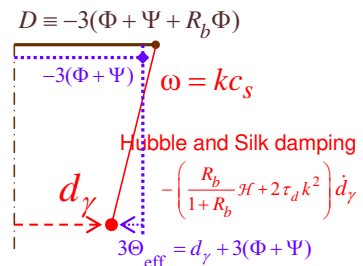


FIG. 3.— An accurate mechanical analogy for general-relativistic evolution (2) of an acoustic CMB mode. The CMB overdensity  $d_\gamma$  equals the denoted distance to the tip of a pendulum with an internal frequency  $\omega = kc_s$  and its suspension point driven as specified by the gravitational driving term  $D$ , eq. (4). For adiabatic initial conditions the evolution starts with  $d_{\text{in}} = 3\zeta_{\text{in}}$ , where  $\zeta_{\text{in}}$  is the superhorizon value of the Bardeen curvature. In the radiation era, initially,  $D_{\text{in}} = \frac{4}{3}(1 + \frac{1}{2}R_\nu)/(1 + \frac{4}{15}R_\nu)d_{\text{in}}$  and in the matter era  $D_{\text{in}} = \frac{6}{5}d_{\text{in}}$  (Bashinsky & Seljak 2004), c.f. Figs. 1 and 4. The advantages of this approach over considering  $\delta T^{(\text{New})}/T$  or  $\Theta_{\text{eff}} = \delta T^{(\text{New})}/T + \Phi = \frac{1}{3}d_\gamma + \Phi + \Psi$  as independent dynamical variables include: (A) Independence of the gravitational force that drives  $\dot{d}_\gamma$  from  $\dot{d}_\gamma$  itself. (B) Epoch- and scale-independence of the relation between the superhorizon perturbation  $d_{\text{in}}$  and the inflation-generated conserved curvature  $\zeta_{\text{in}}$  ( $d_{\text{in}} = 3\zeta_{\text{in}}$ ). (C) Direct cause-effect connection between local physical dynamics and the apparent changes of the variable that describes CMB perturbations.

$\Phi + \Psi$  at the respective epochs is very similar.

#### Coupled regime ( $z \gtrsim z_{\text{rec}} \sim 1100$ )

Any CMB mode prior to recombination evolves according to eq. (2) of a driven damped harmonic oscillator. Fig. 3 presents an equivalent mechanical system—a pendulum whose evolution is described by the same equation. The pendulum’s internal frequency is  $kc_s$  and its pivot is moved by a distance

$$D = -3(\Phi + \Psi + R_b\Phi). \quad (25)$$

The CMB overdensity  $d_\gamma(\tau)$  then numerically equals the distance to the pendulum’s tip, as marked on the figure. To account for the Hubble and Silk damping, the pendulum may be imagined submerged in a viscous fluid with appropriate time-dependent viscosity. All the influence of the metric per-

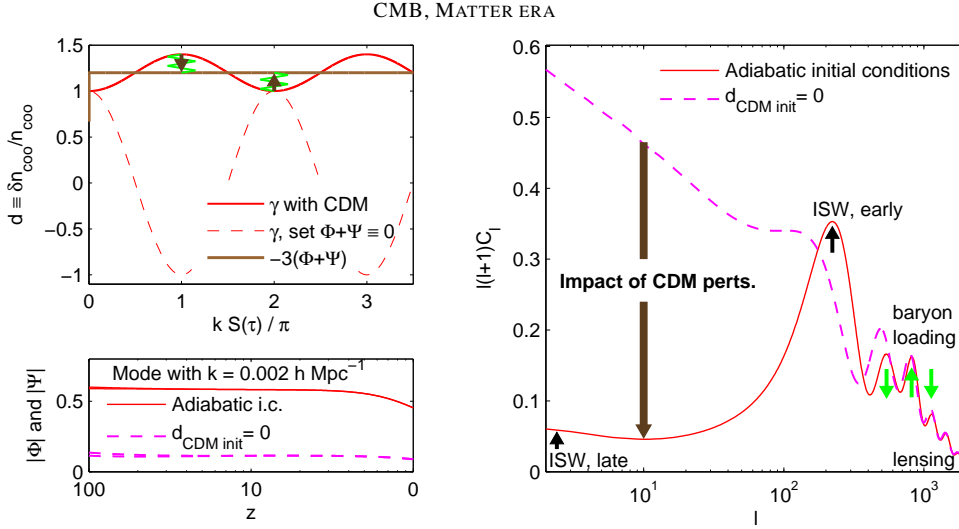


FIG. 4.— Gravitational suppression of CMB temperature anisotropy by growing cosmic structure in the matter era (5-fold for  $\Delta T/T$ , 25-fold for power  $C_l$ ). — Left top: Evolution of  $d_\gamma$  and the driving term  $D$  during matter domination with  $R_b$  set negligible (solid). Evolution of  $d_\gamma$  from the same primordial perturbation if the metric becomes homogeneous before the horizon entry (dashed). — Right: Suppression of the CMB temperature power  $C_l$  for  $l \lesssim 100$  by CDM inhomogeneities. The solid curve describes the same model with changed initial CDM perturbations:  $d_{\text{CDM}}$  is artificially set to zero on superhorizon scales (the superhorizon  $d_\gamma$ ,  $d_\nu$ , and  $d_b$  are unchanged). Then CDM inhomogeneities and the associated potential in the matter era are reduced. The smoother metric suppresses the CMB power at  $l \lesssim 100$  less, as the  $C_l$  plots (obtained with CMBFAST) clearly show. — Left bottom: The plots of  $\Phi$  and  $\Psi$  transfer functions confirm that the last model has smaller  $\dot{\Phi} + \dot{\Psi}$ , hence, the enhancement of its power at low  $l$  cannot be attributed to the ISW effect.

turbations on  $d_\gamma$  is transferred through the (generally, time-dependent) position of the pendulum's pivot  $D(\tau)$ .

This mechanical analogy of the acoustic CMB evolution makes intuitive the following important facts: Foremost, the CMB overdensity is influenced strongly by the *values* of the potentials at horizon entry. Also, as already observed in Sec. 5.2, the sensitivity and even the sign of the CMB response to the subsequent changes of the potentials depend strongly on the *time* and *duration* of the change.

When at horizon entry the driving term  $D$  is close to the superhorizon value of  $d_\gamma$  (as it usually is for adiabatic perturbations) and when  $D$  *does not decay quickly* during the entry then CMB temperature anisotropy is suppressed dramatically. For a specific example, roughly reflecting the evolution between radiation-matter equality and decoupling ( $3 \times 10^3 > z > 1 \times 10^3$ ), let us ignore the baryon-photon ratio  $R_b$  by taking  $D \simeq -3(\Phi + \Psi)$ . Let us evaluate the potentials in a CDM-dominated limit, in which  $\Phi(\tau) = \Psi(\tau) = \text{const} = -\frac{1}{5}d_{\text{in}}$ , where for adiabatic perturbations  $d_{\text{in}} \equiv d_a(\tau \rightarrow 0) = 3\zeta(\tau \rightarrow 0)$  for all species  $a$ .<sup>12</sup> In these approximations,

$$D(\tau) = \frac{6}{5}d_{\text{in}}, \quad (26)$$

being time-independent during and after the mode entry. Then the amplitude of acoustic CMB oscillations is *suppressed 5-fold* (Bashinsky 2006), which is evident from Fig. 3 or the left top panel of Fig. 4.

After the entry, a slow variation of  $D$  over a characteristic time  $\delta\tau$  that exceeds the period of  $d_\gamma$  oscillations ( $\delta\tau k \gg 1$ ) has minor impact on the oscillation amplitude and phase. In particular, this impact vanishes in the adiabatic limit,  $\delta\tau k \rightarrow \infty$ . A typical temporal scale of linear variations of  $\Phi$  and  $\Psi$ , and so of  $D$ , is  $\delta\tau \sim \mathcal{H}^{-1}$ . This applies even to subhorizon scales,

<sup>12</sup> The CDM-domination result  $\Phi = \Psi = -\frac{1}{5}d_{\text{in}}$  follows straightforwardly from eqs. (7, 11-12) and from  $\Phi = \Psi$  by eq. (14). It is also easy to derive from the known relation between potentials and the traditional proper overdensity by remembering that for pressureless matter  $d = \delta\rho/\rho - 3\Psi$ .

where only the perturbations with negligible pressure, hence no rapid internal oscillations, contribute to the potentials. Thus deeply *subhorizon* CMB modes (for which  $\delta\tau k \sim k/\mathcal{H} \gg 1$ ) are *insensitive* to such variations. Conversely, the modes that are closer to horizon entry are affected more strongly.

#### Streaming regime ( $z \lesssim z_{\text{rec}} \sim 1100$ )

Analogous results exist for the sensitivity of the CMB to gravitational potentials after recombination.

When the universe is matter-dominated and baryons have decoupled from the CMB ( $10^3 > z \gg 1$ ) then  $\Phi$  and  $\Psi$  are equal and time-independent on all scales that are sufficiently large to evolve linearly and to be unaffected by the residual baryonic pressure. For time-independent  $\Phi + \Psi$  and negligible collision term  $C_T$  in eq. (5), an “effective” CMB intensity perturbation

$$l_{\text{eff}} \equiv l + 4(\Phi + \Psi) \quad (27)$$

is constant along the line of sight (Kodama & Sasaki 1986; Hu & Sugiyama 1994, 1995). Under a general evolution of the potentials, eq. (5) gives

$$\dot{l}_{\text{eff}} + n_i \nabla_i l_{\text{eff}} = 4(\dot{\Phi} + \dot{\Psi}) + C_T. \quad (28)$$

Prior to horizon entry, the intensity perturbation  $l$  is frozen and equals  $l_{\text{in}} = \frac{4}{3}d_{\gamma, \text{in}}$  (see Bashinsky 2006). As discussed earlier, for the modes that enter during the domination of pressureless matter,  $\Phi(\tau) = \Psi(\tau) = -\frac{1}{5}d_{\text{in}}$ . Then, for adiabatic perturbations for which  $d_{\gamma, \text{in}} = d_{\text{in}}$ , eq. (27) gives

$$l_{\text{eff}} = -\frac{1}{5}l_{\text{in}}. \quad (29)$$

Similarly to the CMB evolution in the coupled regime, for most of these modes the late ISW effect due to the *slow* decay of the potentials at  $z \lesssim 1$  does not noticeably change  $l_{\text{eff}}$ .<sup>13</sup> Thus, first, the presently observed temperature anisotropy in the

<sup>13</sup> The solution of the transport equation (28) for a perturbation mode  $l_{\text{eff}} =$

considered modes is suppressed by the potentials of the clustering matter 5-fold<sup>14</sup>—suppressed with respect to a fictitious scenario in which in the matter era  $\Phi = \Psi = 0$ , consequently,  $t_{\text{eff}} = t_{\text{in}}$ . Second, after decoupling as well, the primary CMB anisotropies have little sensitivity to the potentials’ evolution on subhorizon scales.

The 5-fold suppression is a physical effect, independent of the choice of variables or gauge. It is absent in models where the matter-era potentials decay early during horizon entry or where the laws of gravity are modified so that matter inhomogeneities do not perturb the metric. Note that if all modes that contribute to the CMB temperature autocorrelation  $C_\ell$  at some  $\ell$  are suppressed 5-fold then the  $C_\ell$  is suppressed by  $5^2 = 25$  times.

The right panel of Fig. 4 presents convincing evidence for the reality of the order-of-magnitude suppression of the CMB temperature power spectrum at low  $\ell$ ’s by dark matter clustering. The plot shows the CMB temperature power spectra  $C_\ell$  obtained with a modified CMBFAST code (Seljak & Zaldarriaga 1996) for two models both of which have the identical matter content of the concordance  $\Lambda$ CDM model (Spergel et al. 2006; Seljak et al. 2006; Tegmark et al. 2006). The models differ only by the initial conditions for CDM perturbations. In one of the models (solid curve) all species are initially perturbed adiabatically. In the other model (dashed curve) the CDM density perturbation  $d_c$  is artificially set to zero on superhorizon scales while the initial values for  $d_\gamma$ ,  $d_\nu$ , and  $d_b$  are unchanged. As a consequence, in the second model the metric inhomogeneities in the matter era are reduced. While this model has a smaller ISW effect (see the left bottom panel of Fig. 4), due to the smoother metric, its CMB power for  $\ell \lesssim 100$  is considerably larger.

The suppression of the CMB anisotropy on large scales, which enter during matter domination and active growth of structure, should not be partly traded for the “resonant self-gravitational driving” of small-scale modes that enter in the radiation era. The acoustic modes entering during radiation domination are often said to be resonantly driven by a specially timed decay of their self-generated potential. In reality, the suppression of large relative to small scales is not very sensitive to the timing of the potential decay in the radiation era (Bashinsky 2006). Moreover, the same (when accounting for neutrinos, even somewhat larger) suppression of large relatively to small scales would be observed if in the radiation era the metric were unperturbed, hence, the small-scale modes objectively could not be driven gravitationally (Bashinsky 2006).

#### 5.4.3. Quantifying the response of the CMB power spectrum

$A(\tau) e^{i\mathbf{k}\cdot(\mathbf{x}-\mathbf{n}\tau)}$  in a potential  $\Phi + \Psi = F(\tau) e^{i\mathbf{k}\cdot\mathbf{x}}$  is

$$A(\tau) = A_{\text{in}} + 4 \int_0^\tau \dot{F}(\tau') e^{i\mathbf{k}\cdot\mathbf{n}\tau'} d\tau'. \quad (30)$$

Due to the oscillating factor  $e^{i\mathbf{k}\cdot\mathbf{n}\tau'}$ , any slow variation of the subhorizon potential over a temporal scale  $\delta\tau$  does not affect any modes except for those few with  $|\mathbf{k}\cdot\mathbf{n}|\delta\tau \lesssim 1$ , i.e., those whose wavevector is nearly orthogonal to the direction of light propagation.

<sup>14</sup> This suppression, by a factor of 5, is larger than an apparent factor of 2 suppression that is usually inferred, erroneously, from the traditional description of the Sachs-Wolfe effect in terms of the proper Newtonian-gauge perturbations. (Indeed, for the latter  $\Delta T/T|_{\text{observed}} \simeq -\frac{1}{2}(\delta T^{(\text{Newt})}/T)_{\text{decoupling}}$ , assuming matter domination at decoupling. Yet this result is specific to the Newtonian gauge condition for the decoupling surface, on which the considered perturbations are superhorizon. It should not be given its traditional physical interpretation directly.) See Bashinsky (2006) for additional discussions.

The CMB sensitivity to gravitational potentials at various epochs can be quantified as follows. The temperature anisotropy of CMB radiation observed in a direction  $\mathbf{n}$  is given by the following integral along the line of sight (Seljak & Zaldarriaga 1996):

$$\frac{\Delta T(\mathbf{n})}{T} = \int_0^{\tau_0} d\tau S(\tau, \mathbf{n}r(\tau)). \quad (31)$$

Here,  $\tau_0$  is time at present,  $r(\tau) = \tau_0 - \tau$  (in flat models) is the radial distance along the line of sight, and the source equals

$$S = \dot{g} \left( \frac{1}{3} d_\gamma + \Phi + \Psi - v_b^i n_i + Q^{ij} n_i n_j \right) + g \left( \dot{\Phi} + \dot{\Psi} \right), \quad (32)$$

with  $v_b^i$  being the baryon velocity,  $Q^{ij}$  being determined by the radiation quadrupole and polarization, and a visibility function  $g(\tau) = \exp(-\int_\tau^{\tau_0} d\tau/\tau_T)$  giving the probability of CMB photons to reach us unscattered. Regardless of the random realization of the primordial curvature perturbation  $\zeta_{\text{in}}$ , the physics behind the subsequently developed perturbations of potentials, densities, etc. in linear theory can be described by transfer functions

$$T_\Phi(k, \tau) \equiv \Phi(k, \tau)/\zeta_{\text{in}}(k), \quad (33)$$

with analogous definitions for other scalar perturbations:  $\Psi$ ,  $d_\gamma$ , velocity potential  $u_b$  (s.t.  $v_b^i = -\partial_i u_b$ ), etc.

The CMB constraints on the transfer functions are derived from observational estimates of CMB angular power spectra  $C_\ell$ . In particular, the temperature power spectrum equals (Seljak & Zaldarriaga 1996)

$$C_\ell = 4\pi \int_0^\infty \frac{dk}{k} \Delta_\zeta^2(k) \left| \int_0^{\tau_0} d\tau T_S(\tau, k) j_\ell(kr(\tau)) \right|^2, \quad (34)$$

where  $\Delta_\zeta^2(k) \equiv k^3 P_\zeta(k)/(2\pi^2)$  is the dimensionless primordial power of  $\zeta_{\text{in}}(k)$ , and  $j_\ell$  is the spherical Bessel function. In eq. (34), the full transfer function  $T_S$  of the source  $S$ , eq. (32), is a differential operator, with derivatives corresponding to the direction-dependent terms of  $S$ . In the following discussion we will mostly be concerned with its scalar terms, as only they involve the gravitational potentials directly.

It is useful to keep in mind that the dominant contribution to  $C_\ell$  at a given  $\ell$  comes from the modes with  $k \sim \ell/r$ . Indeed,  $j_\ell(kr)$  vanishes exponentially at smaller values of  $k$  and as  $1/k$  at higher values.

#### Radiation era ( $z > z_{\text{eq}} \sim 3000$ , probed by $\ell > 200$ )

By the arguments of Sec. 2, only the modes that enter the horizon before radiation-matter equality provide information about the metric and dark dynamics in the radiation era. Then after horizon entry  $\delta\rho/\rho \approx \delta\rho_\gamma/\rho_\gamma$  oscillates with nearly constant amplitude. Consequently, the induced  $\Phi + \Psi$  decays as  $\tau^{-2} \propto a^{-2}$  [eq. (1)]. Although the potential decay is eventually halted by the growth of structure since matter domination,  $\Phi + \Psi$  for these modes remains a subdominant source of CMB anisotropy in eq. (32), exceeded by the intrinsic photon-baryon perturbations.<sup>15</sup>

Thus the impact of gravitational potentials in the radiation era is confined to horizon entry. It is fully encoded in the amplitude and phase of the subsequent acoustic oscillations. Specific cases of such an impact were considered in Secs. 5.1 and 5.2.

<sup>15</sup> Photon-baryon perturbations also decay on small scales due to Silk damping. Estimates (Hu & Sugiyama 1996; Weinberg 2002) show that the exponential Silk damping overcomes the quadratic decay of the potential only at  $\ell \gtrsim 4000$ , where secondary anisotropies are expected to dominate the considered primary signal.

*From equality to recombination* ( $z_{\text{rec}} < z < z_{\text{eq}}$ ,  $100 < \ell < 200$ )

The CMB modes that enter during and after radiation-matter equality ( $z_{\text{eq}} \sim 3000$ ) oscillate in a significant gravitational potential of growing matter inhomogeneities. Close to  $z_{\text{eq}}$ , the driving potential  $\Phi + \Psi$  still evolves appreciably. The potential continues to decay because of the residual radiation density. It decays until recombination ( $z_{\text{rec}} \approx 1100$ ) also due to coupling of the baryonic component of matter to the CMB, slowing the structure growth by excluding the baryons from it (e.g., Hu & Sugiyama 1996).

Altogether, these effects lead to complicated evolution of the modes that enter during  $z_{\text{rec}} < z < z_{\text{eq}}$ . Then both the intrinsic and gravitational terms in the source of  $\Delta T/T$  (32) contribute noticeably. As highlighted by many studies, the term  $\dot{\Phi} + \dot{\Psi}$  in eq. (32) due to the continuing decay of potentials then is also large and boosts the height of the first acoustic peak (early ISW effect).

*After recombination* ( $z < z_{\text{rec}} \simeq 1100$ , probed by  $\ell < 100$ )

The evolution of linear perturbations becomes simple again when  $z \ll z_{\text{rec}}$ . On the scales that enter at this epoch but before dark energy becomes dynamically relevant, we expect that during linear evolution  $\Phi(\tau) = \Psi(\tau) = -\frac{1}{5}d_{\text{in}} = \text{const}$  (footnote 12). The presently observed perturbation of CMB intensity for almost all these modes is suppressed 5-fold. Our next goals will be, first, to confirm that the contribution of these modes to  $C_\ell$  is indeed gravitationally reduced by a factor of  $5^2 = 25$ . Second, to find the sensitivity of  $C_\ell$  to different values of potentials due to non-standard physics. And third, to quantify the  $C_\ell$  response to the evolution of potentials on subhorizon scales.

We start from noting that not only do the modes of different  $k$ 's contribute to the correlation function  $C_\ell$  (34) incoherently, but coherence is also lost for same- $k$  contributions at widely separated times,  $|\tau - \tau'|k \gg 1$ . To see this explicitly, we rewrite eq. (34) as

$$C_\ell = 4\pi \int \frac{dk}{k} \Delta_\zeta^2(k) \int d\tau T_S(\tau, k) \int d\tau' T_S^*(\tau', k) p_\ell(kr, kr'). \quad (35)$$

The last factor  $p_\ell(kr(\tau), kr(\tau'))$  describes the kernel of projecting the harmonic plane-wave modes on a spherical multipole  $\ell$

$$p_\ell(x, x') \equiv j_\ell(x)j_\ell(x'). \quad (36)$$

This function for  $\ell = 10$ , as an example, is shown in Fig. 5.

In the integrand of eq. (35), except for very low redshifts,  $p_\ell(kr, kr')$  varies with  $k$  much more rapidly than  $T_S(\tau, k)$  and  $T_S^*(\tau', k)$ .<sup>16</sup> With  $T_S$ ,  $T_S^*$ , and  $\Delta_\zeta^2(k)$  almost unchanged over many  $k$  periods of the  $p_\ell$  oscillations, we can see from Fig. 5 that positive and negative contributions to  $\int (dk/k) p_\ell(kr, kr')$  mutually cancel whenever

$$|\tau - \tau'| = |r - r'| \gg 1/(\text{contributing } k). \quad (37)$$

Thus the contributions to  $C_\ell$  from sources at this temporal separation are incoherent. In particular, we can ignore the coherence of, and study independently, the contributions to  $C_\ell$  at the horizon entry ( $\tau \lesssim 1/k$ ) and during subhorizon evolution ( $\tau \gg 1/k$ ).

First, we consider a time interval from  $\tau = 0$  to  $\tau_{\text{ent}} \sim 1/k$ . For a mode that enters at any time after recombination, the

<sup>16</sup> The characteristic scales of variation are  $\Delta k \sim \min(r^{-1}, r'^{-1})$  for  $p_\ell$ , versus  $\Delta k \sim \tau^{-1}$  and  $\tau'^{-1}$  for  $T_S$  and  $T_S^*$  respectively.

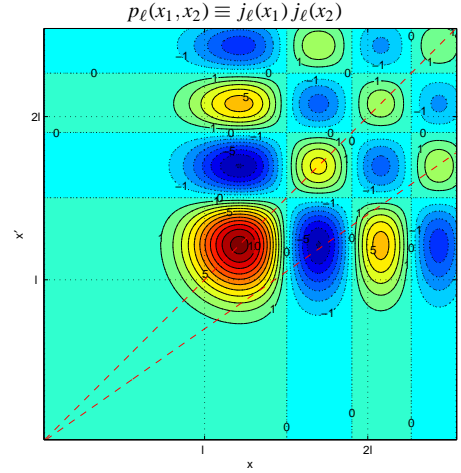


FIG. 5.— The isocontours of the kernel  $p_\ell(x_1, x_2) \equiv j_\ell(x_1)j_\ell(x_2)$  of projecting perturbation  $k$ -modes to  $C_\ell$ , eqs. (35, 36). The figure is for  $\ell = 10$ . The labels on the contours show the values of  $p_{10}/10^{-3}$ . Note that  $p_\ell(x_1, x_2) \approx 0$  whenever either  $x_1 < \ell$  or  $x_2 < \ell$ . Also note that  $p_\ell \geq 0$  along the line  $x_1 = x_2$  (diagonal dashed line), but  $p_\ell$  oscillates through positive and negative values along any line  $x_1 = cx_2$  with  $c \neq 1$  (e.g., lower dashed line).

source (32) forms a complete derivative:<sup>17</sup>

$$S \approx \frac{\partial}{\partial \tau} \left[ g \left( \frac{1}{3}d_{\gamma, \text{in}} + \Phi + \Psi \right) \right]. \quad (38)$$

Starting from eq. (34), neglecting the change of  $j_\ell(kr(\tau))$  over the considered time interval  $(0, \tau_{\text{ent}})$ , and trivially integrating the complete derivatives (38) over  $d\tau$  and  $d\tau'$ , we obtain

$$\delta C_\ell^{(\text{postrec entry})} \approx 4\pi \int \frac{dk}{k} \Delta_\zeta^2(k) j_\ell^2(kr) \left| g \left( \frac{1}{3}d_{\gamma, \text{in}} + \Phi + \Psi \right) \right|_{\text{entry}}^2 \quad (39)$$

where the variables  $d_{\gamma, \text{in}}$ ,  $\Phi$ , and  $\Psi$  now stand for the corresponding transfer functions, normalized by the condition  $\zeta(\tau \rightarrow 0, k) \equiv 1$ . When the primordial power is nearly scale invariant, we can neglect the  $k$ -dependence of  $\Delta_\zeta^2(k)$  over the range of  $k \sim \ell/r$  that contribute to the integral (39). We can also ignore the variation of the transfer functions in the last parentheses over this range. Integration of the remaining  $k$ -dependent terms by the standard formula  $\int \frac{dx}{x} j_\ell^2(x) = [2\ell(\ell+1)]^{-1}$  gives

$$\delta C_\ell^{(\text{postrec entry})} \approx \frac{2\pi \Delta_\zeta^2(\ell/r_{\text{ent}})}{\ell(\ell+1)} \left| g \left( \frac{1}{3}d_{\gamma, \text{in}} + \Phi + \Psi \right) \right|_{\text{entry}}^2. \quad (40)$$

Eqs. (39) or (40) quantify the response of  $C_\ell$  to the gravitational potentials at horizon entry after recombination. These equations confirm that for adiabatic perturbations that enter in the matter era the potentials  $\Phi = \Psi = -\frac{1}{5}d_{\text{in}}$  suppress the corresponding contribution to  $C_\ell$  25-fold.

We now consider the response of  $C_\ell$  to changes of potentials on subhorizon scales. Then the CMB sensitivity can be quantified in the Limber approximation (Limber 1954), applied to the CMB by Kaiser (1984, 1992) and Hu & White (1996). With the details of the calculation given in Appendix A, the response of the power spectrum of CMB temperature to subhorizon changes of potentials is roughly

$$\delta C_\ell^{(\text{postrec subhor.})} \sim \frac{2\pi^2 \Delta_\zeta^2(\ell/r)}{\ell^2} [\delta(\Phi + \Psi)]^2 \frac{r}{\ell \delta \tau}. \quad (41)$$

<sup>17</sup> For such modes,  $g$  significantly deviates from zero only when the mode is superhorizon. Then the factor that multiplies  $g$  in the full source (32) reduces to  $(\frac{1}{3}d_{\gamma, \text{in}} + \Phi + \Psi)$ , giving eq. (38).

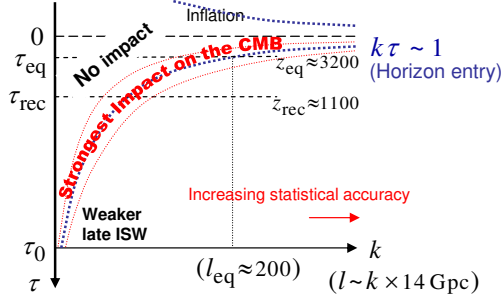


FIG. 6.— While the acoustic pattern of CMB temperature anisotropy is formed on the surface of last scattering ( $z_{\text{rec}} \sim 1100$ ), the metric perturbations on this surface *do not play a major role* in the observed CMB spectra  $C_\ell$ . The potentials at last scattering do control the subdominant “baryon loading” effect. Primarily, however, the CMB multipoles are sensitive to the gravitational potentials and underlying dark dynamics at the *horizon entry* of the corresponding modes ( $z \sim \ell^2/4$  for  $z < z_{\text{eq}}$ , and  $z \sim 20\ell$  for  $z \gtrsim z_{\text{eq}}$ ), covering the entire range from  $z \sim 1$  for lowest  $\ell$  up to  $z \sim 6 \times 10^4$  for  $\ell \sim 3000$ .

Here  $r$  is the comoving radial distance to the changing potentials and  $\delta\tau$  is the time taken by a change  $\delta(\Phi + \Psi)$ , assumed gradual.

Even for large changes of potentials ( $|\delta(\Phi + \Psi)| \sim |\Phi + \Psi|$ ) the observed response  $\delta C_\ell^{\text{(subhor.)}}$  (41) is suppressed relative to  $C_\ell^{\text{(entry)}}$  (40) by a factor  $\frac{r}{\ell\delta\tau}$ . We argued previously that under linear evolution generally  $\delta\tau \sim \mathcal{H}^{-1}$ . Then for subhorizon scales ( $r/\ell \ll \mathcal{H}^{-1}$ ) the factor  $\frac{r}{\ell\delta\tau}$  is much smaller than unity. This suppression is easily understood as the cancellation of positive and negative contributions to  $\Delta T/T$  from the peaks and troughs of all perturbation modes except for those whose  $\mathbf{k}$  is almost orthogonal to the line of sight (Hu & White 1996).

In addition, dark dynamics influences the CMB indirectly through the gravitational impact on baryons, coupled to the CMB by Thompson scattering. After recombination, the baryon-mediated linear contribution on subhorizon scales is suppressed even more than the late ISW contribution (41). Indeed, the direct contribution of baryon velocity  $v_b^i n_i$  to the source of CMB temperature perturbation (32) in the Limber limit vanishes (Hu & White 1996): In this limit, only the modes with  $\mathbf{k}$  orthogonal to  $\mathbf{n}$  would contribute to  $C_\ell$ , yet for their scalar perturbations (with  $v^i$  parallel to  $\mathbf{k}$ )  $v_b^i n_i = 0$ . The indirect effect of weakly coupled baryonic perturbations through affecting the photon overdensity or other photon multipoles in the source (32) is also diminished relative to the already suppressed ISW term by an additional factor  $\delta\tau/\tau_T$ , where  $\tau_T$  is the photon free-flight time. This factor is small for any temporal interval after CMB decoupling.

The CMB is also affected through various non-linear effects, e.g., its lensing by cosmic structure or Sunyaev-Zeldovich effect. Unlike the primary anisotropies, these non-linear features may be useful probes of the dark dynamics on small scales whenever they can be separated from the dominant primary signal (e.g., Seljak & Zaldarriaga 1999; Hu & Okamoto 2002).

### Overall

The above results can be summarized concisely as follows. At a given comoving scale  $k$ , probed by  $\ell \sim kr \approx k \times 14 \text{ Gpc}$ , the CMB anisotropy is most sensitive to the value and evolution of  $\Phi + \Psi$  during the scale’s horizon entry. This is illustrated by Fig. 6. Although most of the observed CMB photons scattered last during hydrogen recombination at  $z_{\text{rec}} \sim 1100$ , the poten-

tials during recombination are of relatively minor importance for the observed anisotropies. (Exceptions are the scales of the first peak that happened to enter during recombination, and the nondegenerate baryon-loading signature on smaller scales.)

When the potentials do not decay quickly during the entry, they significantly suppress the CMB temperature spectrum  $C_\ell$  (by a factor of 25 in the Einstein-de Sitter scenario with adiabatic perturbations.) The  $C_\ell$  response to changes of the potentials after the entry is weak. After recombination, in particular, the  $C_\ell$  response to the subhorizon changes of potentials is diminished by a factor  $\sim \mathcal{H}/k$ .

In principle,  $\Delta T/T$  of the CMB responds comparably well to the metric inhomogeneities during the horizon entry at either high or low redshifts. Nevertheless, the CMB is a considerably better probe of the horizon-scale potentials at high redshifts because of the reduced cosmic variance. Let us define the wavevector  $k_{\text{ent}}$  of the CMB modes that enter at a redshift  $z$  by a condition  $k_{\text{ent}} S(z) \equiv 1$ , where  $S = \int c_s d\tau$  is the corresponding size of acoustic horizon. The modes that enter at a redshift  $z$  match to the multipole  $\ell_{\text{ent}} = k_{\text{ent}} r = r/S$ . Taking  $S \approx \tau/\sqrt{3}$  as a valid estimate both in the radiation era (when  $R_b$  is negligible) and after recombination (when baryons decouple and formally  $c_{\text{eff},\gamma}^2 = 1/3$ ), we obtain

$$\ell_{\text{ent}}(z) \equiv \frac{r}{S} \approx \begin{cases} z/18, & \text{radiation era,} \\ \sim 2\sqrt{z}, & \text{matter era,} \end{cases} \quad (42)$$

estimated for a  $\Lambda$ CDM model with  $\Omega_m h^2 = 0.13$  and  $h = 0.7$ . For this model the redshift of equality  $z_{\text{eq}} \approx 3110$  and recombination  $z_{\text{rec}} \approx 1090$  match to  $\ell_{\text{ent}} \approx 200$  and 90 respectively.

The  $1\text{-}\sigma$  uncertainty of probing a non-degenerate effect, quantified by a parameter  $p$ , can be evaluated as (e.g., Kendall & Stuart 1979)

$$\Delta p = 1 / \sqrt{\sum_i \left( \frac{\partial C_i / \partial p}{\text{r.m.s. } C_i} \right)^2}. \quad (43)$$

For a CMB experiment limited on the studied scales only by cosmic variance, for either temperature or polarization power spectra ( $\text{r.m.s. } C_i / C_i = [(\ell + \frac{1}{2}) f_{\text{sky}}]^{-1/2}$  (Knox 1995; Seljak 1996; Zaldarriaga et al. 1997), where  $f_{\text{sky}} \leq 1$  is the experimental sky coverage. Then

$$\Delta p = 1 / \sqrt{\sum_i (\ell + \frac{1}{2}) f_{\text{sky}} \left( \frac{\partial \ln C_i}{\partial p} \right)^2}. \quad (44)$$

Thus for constraining an effect that affects the modes which enter the horizon at a redshift  $z$  over a span of redshifts  $\Delta z$ , by eq. (42), we can expect accuracy

$$\Delta p \sim f_{\text{sky}}^{-1/2} (\partial \ln C_i / \partial p)^{-1} \times \begin{cases} 18 / \sqrt{z \Delta z}, & \text{radiation era,} \\ 1 / \sqrt{2 \Delta z}, & \text{matter era.} \end{cases} \quad (45)$$

This accuracy improves with increased  $\Delta z$  and, when probing the radiation era, with increased  $z$ .

## 6. APPLICATIONS AND CAVEATS FOR MODIFIED GRAVITY

We now briefly consider the possibility that general relativity (GR) breaks down on cosmological scales. Modified gravity (MG) offers rich phenomenology by invoking new degrees of freedom whose dynamics is substantially different and often involves more parameters than the standard cosmological model. It typically predicts nonstandard evolution of perturbations on horizon and subhorizon scales alike.

While the detection of such phenomena as non-standard growth of cosmic structure or anomalous lensing may indicate MG, we will see that without any restrictions on the dark dynamics, the identical effects could always be generated by a non-minimal dark sector that influences the visible matter according to the standard Einstein equations.<sup>18</sup> Further in this section we will argue that other features should yet allow to discriminate MG observationally.

We will assume that even if full Einstein gravity fails on cosmological scales, the Einstein principle of equivalence remains valid for the visible species. This assumption is common to many existing MG models. It is motivated by the relatively strong terrestrial and solar-system constraints on the equivalence principle.

Thus we suppose that the regular matter couples covariantly to a certain matter-frame “physical” metric  $g_{\mu\nu}$ . However, we now neither take for granted that all dark fields also couple covariantly to the same metric  $g_{\mu\nu}$ , nor assume that the dynamics of  $g_{\mu\nu}$  itself is governed by the Einstein equations.

Under the weaker assumption of the equivalence principle for only the visible matter, all observable signatures of new physics can still be quantified by *any of the three parameterization schemes* of Sec. 4. Indeed, the  $g_{\mu\nu}$  background can still be described by a single number for its present spatial curvature and by its uniform redshift-dependent expansion rate  $\mathcal{H}(z)$ . The potentials  $\Phi$  and  $\Psi$ , defined by eq. (3) to parameterize the inhomogeneities of the physical metric  $g_{\mu\nu}$ , will play their usual role in the evolution of light and baryons. Moreover, the (effective dark) energy and momentum densities assigned to the missing sources of curvature by the naive application of the Einstein equations will evolve in agreement with the usual local conservation laws, which is easily seen as follows.

Let by definition

$$T_{\text{eff dark}}^{\mu\nu} \equiv \frac{1}{8\pi G} G^{\mu\nu} - \sum_{\text{known } a} T_a^{\mu\nu}, \quad (46)$$

where the last sum is over the known regular particles. Their energy-momentum tensor [constructed unambiguously from the species’ action  $S_a$  as  $T_a^{\mu\nu} = (2/\sqrt{-g}) \delta S_a / \delta g_{\mu\nu}$ ] is covariantly conserved by the assumed covariance for the regular species. The matter-frame Einstein tensor  $G_{\mu\nu} = R_{\mu\nu} - \frac{1}{2} g_{\mu\nu} R$ , where  $R_{\mu\nu}$  is the Ricci tensor of the physical metric, is also covariantly conserved by the Bianchi identities. Thus the entire expression (46) is covariantly conserved:

$$T_{\text{eff dark};\nu}^{\mu\nu} = 0, \quad (47)$$

with all covariant derivatives being taken relative to the physical metric.

Since  $T_{\text{eff dark}}^{\mu\nu}$  is covariantly conserved, the background and perturbations of the missing energy and momentum evolve according to equations (16) – (19), derived from the identical conservation law. Thus if all our probes of the invisible degrees of freedom are based solely on their gravitational impact on light, baryons, and other regular particles (neutrinos, WIMP’s when probing dark energy, etc.) then phenomenologically *all observable signatures* of a considered MG model can be mimicked by an effective GR-coupled dark sector. Specifically, we can find the corresponding effective  $w(z)$  to reproduce the missing energy background, and the effective anisotropic stress  $\sigma(z, k)$  and stiffness  $c_{\text{eff}}^2(z, k)$  to describe scalar perturbations. For ex-

ample, for a popular DGP gravity model (Dvali et al. 2000) this was demonstrated explicitly by Kunz & Sapone (2007).

With this discouraging general conclusion, we may enquire whether cosmology can at all reveal definitive distinctions between MG and general relativity with a peculiar yet physically permissible dark sector. To establish such distinctions, let us summarize the conceptual differences of MG from general relativity:

- A. Some dark degrees of freedom may not couple covariantly to the matter metric  $g_{\mu\nu}$ .
- B. The gravitational action may not be given entirely by the Hilbert-Einstein term  $S_{\text{grav}} = (16\pi G)^{-1} \int d^4x \sqrt{-g} R$ .

The distinctive observable consequences of these special properties of MG may include:

1. The effective dark dynamics, which is observationally inferred by assuming the Einstein equations, violates the equivalence principle (EP). The EP violation can be seen, e.g., as
  - i. The dependence of the inferred local dark dynamics on the distribution of visible matter, when it cannot be explained by non-gravitational dark-visible coupling allowed by particle experiments.
  - ii. Superluminality of the inferred dark dynamics.
2. The dynamics of gravitational waves (tensor modes) deviates from the predictions of the Einstein equations, assuming that both the visible and inferred dark species contribute to the energy-momentum tensor in the simplest way.

Most of these signatures have already been utilized for falsifying MG models with existing or suggested observations, (Clowe et al. 2006; Bradač et al. 2006) and (Kahya & Woodard 2007); we comment additionally on them next.

### 6.1. EP violation for the inferred dark dynamics

The violation of the first condition can be illustrated by an extreme toy theory in which the regular matter (“baryons,” for short) constitute all independent degrees of freedom. Let the metric in this theory be specified by baryon distribution via some deterministic relation (e.g., as  $g^{\mu\nu} = \Lambda^{-1} T_{\text{baryon}}^{\mu\nu}$ , following from an action  $S = S_{\text{baryon}} - \int d^4x \sqrt{-g} \Lambda$  with  $\Lambda$  being a constant). Even in such a contrived theory, by the above arguments, the effective missing energy and momentum densities (46) would appear to evolve and gravitate in agreement with energy-momentum conservation and the Einstein equations. In this example, however, the effective dark density and stress are uniquely determined by the distribution of the visible matter. This does not occur for truly independent dark degrees of freedom.

In more realistic MG theories we should not expect a deterministic relation between the visible and effective dark distributions. Still, if the dark and visible sectors interact other than by coupling covariantly to the common metric then the inferred laws of the effective local dark dynamics would depend on the visible environment.

Detection of such dependencies would be particularly feasible for the dark matter, for which there are plentiful observable regions with varying environment: varying in both visible matter density and in its ratio to dark density. In addition

<sup>18</sup> We stress that these features remain useful hints of MG. Since they are even more ubiquitous than the scenarios of modified gravity and may reveal other new physics, they are well worth searching for.

to baryons clumping strongly at low redshifts, the density of all known visible species varies with redshift due to the Hubble expansion. The ratio of visible to dark density is perturbed even on large scales due to dark matter being decoupled from the photon-baryon acoustic oscillations and clustering on its own until recombination. The segregation of dark matter and baryons is even more apparent at late times on the scales of clusters and smaller, becoming almost complete in the famous bullet cluster example (Markevitch et al. 2004; Clowe et al. 2006; Bradac et al. 2006).

In order to test that the standard CDM+GR model accounts for the signatures of dark matter at various redshifts and scales, it is crucial to observe and robustly model the dynamics on a wide range of scales, including the highly non-linear ones. It is also important to utilize complimentary probes, such as baryonic matter (responding to  $\Phi$ ), and the CMB or gravitational lensing (probing  $\Phi + \Psi$ ). Various signatures of dark matter that allow to compare dark matter parameters under different conditions include: the height alteration of the odd and even CMB acoustic peaks due to the CDM potential affecting the coupled baryons before recombination (Hu & Sugiyama 1996), the early ISW enhancement of the first peak (e.g., Hu et al. 1997), the significant suppression of the CMB temperature power  $C_l$  below the first peak (Sec. 5.4.3 and Fig. 4), the linear and nonlinear dynamics of cosmic structure, and the lensing of the CMB and background galaxies by the CDM potential at lower redshifts.

Dark energy (DE) does not trace any visible species at low redshifts, when its density appears almost redshift-independent. DE may track the radiation or matter background at higher redshifts; then its perturbations are not expected to evolve similarly to any of the standard species. (For example, see the evolution of the perturbations of tracking quintessence in the radiation and matter eras on the right panels of Figs. 1 and 2 respectively.) Constraints on the background equation of state  $w$  can rule out specific DE or MG models but do not decisively differentiate between the DE and MG paradigms. Beyond  $w$ , the perturbations of dark energy are likely to be stiff and thus can be constrained only during horizon entry. As discussed previously, the CMB can provide such constraints over a wide range of redshifts, from  $z \sim 1$  up to  $z \sim 10^5$ , becoming much tighter toward higher redshifts (Sec. 5 and Fig. 6).

With the cosmological constant fitting the current data well, the search for *any manifestation* of non-trivial DE or MG dynamics may be the utmost priority for establishing the origin of cosmic acceleration. This includes falsifying the background equation of state  $w(z) \equiv -1$  at low redshifts but by no means is limited to  $w(z)$ . Examples of other searches, which may end up being more fruitful, are: the search for a subdominant non-standard component in the radiation or early matter era (Secs. 5.2 and 5.4), nonstandard growth of cosmic structure (Linder 2005), and nonstandard  $\Phi/\Psi$  (Bertschinger 2006), probed by comparing the CMB or lensing signal with the galaxy and cluster distributions.

### 6.2. Superluminal dark flows

Another possible signature of MG is the superluminal propagation of dark perturbations. The superluminality may be spurious, from our describing MG by a parameterization that assumes general relativity. It may also be real, from the equivalence principle not applying to some dark degrees of freedom.

While numerous observational tests for superluminality can be thought of, here we consider only one specific example. Spu-

rious or real superluminal propagation of (effective) dark inhomogeneities can be constrained by the sensitivity of the CMB acoustic phase to the propagation velocity of dark perturbations (Sec. 5.3). A straightforward Fisher-matrix forecast shows that TT, TE, and especially EE spectra from the future high- $\ell$  CMB experiments, Planck<sup>19</sup> and ACT<sup>20</sup> in particular, will strongly restrict the abundance of any dark component that supports scalar perturbations with  $c_p^2 > 1/3$ , including  $c_p > 1$ .

If  $B$ -polarization of the CMB reveals the signal of relic gravitational waves (Seljak & Zaldarriaga 1997; Kamionkowski et al. 1997), a similar effect in the tensor sector will directly constrain the streaming dark species for which streaming velocity  $c_p$  exceeds the speed of gravitational waves,  $c_{s,\text{grav}}$ . [Indeed,  $c_{p,\nu} > c_{s,\text{grav}}$ , albeit under somewhat different conditions, for the dark matter emulator of Kahya & Woodard (2007), discussed below.] The oscillation amplitude of the gravitational (tensor) modes after horizon entry is noticeably affected by neutrino perturbations (Weinberg 2004). However, the phase shift of the tensor oscillations is strictly forbidden (Bashinsky 2005) when for all species  $c_{p,\text{dark}} \leq c_{s,\text{grav}}$ , as required by GR. If, on the other hand, the velocity of neutrinos or other dark species with non-negligible abundance exceeds  $c_{s,\text{grav}}$  then the arguments of Bashinsky (2005) show that the phase of the tensor BB signal in the CMB will be necessarily shifted.

### 6.3. Nonstandard phenomenology of gravitational waves

An interesting test of a broad class of MG alternatives to dark matter was recently suggested by Kahya & Woodard (2007). They considered the propagation of a fundamental tensor field  $\tilde{g}_{\mu\nu}$  [whose kinetics is governed by  $S_{\text{grav}} = (16\pi\tilde{G})^{-1} \int d^4x \sqrt{-\tilde{g}} \tilde{R}$ ] in any of the model where  $\tilde{g}_{\mu\nu}$  is sourced by the luminous matter alone by the Einstein law

$$\tilde{G}^{\mu\nu} \approx 8\pi G T_{\text{luminous}}^{\mu\nu}. \quad (48)$$

The physical metric  $g_{\mu\nu}$  was set to reproduce the observed gravitational potentials in the vicinity of our galaxy. The knowledge of the other specifics of the MG dynamics was therefore unnecessary. Then Kahya & Woodard (2007) showed that the arrival of the gravitational waves from a cosmological event, e.g. a supernova, is noticeably *delayed* with respect to the arrival of the associated neutrinos and photons.

While the assumption (48), implicit in Kahya & Woodard (2007), incorporates many models it is not generic. For example, it does not apply if

$$\tilde{G}^{\mu\nu} \approx 8\pi \tilde{G} T_{\text{luminous}}^{\mu\nu}, \quad (49)$$

where  $\tilde{G}$  differs from the local value of Newton's gravitational constant  $G$ . Even in the TeVeS model (Bekenstein 2004), motivating (48),  $\tilde{G} \neq G$  strictly, although it is natural to assume that for TeVeS this difference is small (Bekenstein 2004). Yet more generally,  $\tilde{G}$  may depend on the new MG degrees of freedom, e.g., on the scalar field  $\phi$  of tensor-scalar or tensor-vector-scalar models.

In any case, even if eq. (48) fails and the exact prediction for the gravity wave delay by Kahya & Woodard (2007) does not apply, the gravitational waves and neutrinos or photons would still generally propagate with different velocities. Thus the future gravitational wave astronomy can offer robust tests for discriminating GR-coupled dark matter from modified gravity.

<sup>19</sup> <http://www.rssd.esa.int/Planck>

<sup>20</sup> <http://www.physics.princeton.edu/act>

## 7. SUMMARY

### 7.1. Approach

Constraints on the *inhomogeneous* dynamics of the dark sectors are essential to full understanding of their nature. Varying with both redshift and *spatial scale*  $k$ , the observable imprints of dark perturbations provide plentiful information about the dark sectors' local kinetic properties and (self) interactions. This information significantly complements the dark species' background equation of state  $w(z)$ .

Reliable extraction of the information encoded in the dark perturbations is hindered by the indirectness of their, sometimes subtle, gravitational impact on observables. It is also obstructed by the numerous contributions to the observables from other complex multiscale cosmological and astrophysical phenomena. Moreover, controlled repeatable measurements of dark sectors cannot be afforded when the measuring device is the entire observable large-scale universe. Nevertheless, the unavoidable “nuisance” phenomena and contaminations can be counteracted by detailed understanding of the involved physics and by complementary probes of as many independent characteristics of the dark sectors as can be observationally accessed.

For a tractable and systematic study of the dark sectors beyond the background equation of state, we map the local kinetic properties of inhomogeneous dark dynamics at a given redshift to the characteristics of the observed cosmological distributions that can reflect those dark properties. The correct mapping is more likely to be achieved with a description of evolution that is simple and that manifests the objective causal relations explicitly.

The dynamics of gravitationally coupled perturbations of dark and visible species during horizon entry is pivotal to probing the dark inhomogeneities. Then any dynamical species, including dark radiation and all dark energy candidates with  $w \neq -1$ , are necessarily perturbed and leave imprints of their highly specific inhomogeneous kinetics on the observable probes. The contribution of subhorizon perturbations of a given magnitude  $\delta\rho/\rho$  to gravitational potentials is suppressed, as  $\Phi \sim (\mathcal{H}/k)^2 \delta\rho/\rho$ .

On the scales of the horizon and beyond, the apparent gravitational impact of the dark species on the visible ones depends strongly on the description used. In most descriptions, the apparent inhomogeneities of the visible species are changed by the properties that dark species have long *before* and even long *after* the change. This misguides the identification of the observable features that reflect the internal dark properties at specific epochs.

The apparent cause–effect mismatch is, nevertheless, not intrinsic to linearly perturbed cosmological evolution. Within Einstein gravity, the internal local properties of dark species at a past time  $\tau$  affect only the perturbations that had approached or entered the horizon by the time  $\tau$ . The mapping of dark properties to evolutionary changes is unambiguous after horizon entry, when baryonic and photon perturbations are instantaneously impacted by the Newtonian potentials, then reflecting the instantaneous overdensity of visible and dark species. The remaining, confined to the horizon entry, gravitational impact of the dark sectors at a given  $\mathbf{k}$  in linear theory is also unambiguous (Sec. 2).

It is easy to describe the full perturbed linear cosmological dynamics (including that of partly polarized photons, baryons, realistic neutrinos, quintessence, and other particles or fields) by a formalism in which the changes of perturbations in the

visible sectors are concurrent with the local dark properties responsible for these changes (Bashinsky 2006). The resulting description reveals explicitly the objective causal dependencies and enables us to map observable features to local dark properties more reliably than with traditional formalisms, which lack this concurrence. The suggested formalism considers perturbations of canonical rather than proper distributions. It has additional useful technical benefits, for example, note (A) and (B) in the caption of Fig. 3, illustrating the corresponding description of the acoustic CMB modes.

Using this formalism, we relate general properties of dark perturbations to observable features by tracking the gravitationally coupled evolution of dark and visible perturbations. The advantages of such an evolutionary study over black-box computation of observables are twofold: It isolates all observable signatures of the studied phenomena; it also reveals the mechanisms that generate these signatures and allows us to judge the mechanisms' robustness.

### 7.2. Sensitivity of probes

We categorize the primary probes, responding to the dark dynamics through linear evolution, as either “light” or “matter”, Sec. 3. Those of the first type (CMB spectra) probe the trajectories close to null geodesics; of second type (matter transfer functions) respond to the metric along the time-like Hubble-flow worldlines.

Primary CMB anisotropies are highly sensitive to the values and evolution of the potentials *during horizon entry*. They are only mildly affected by the gravitational potentials on subhorizon scales. (The situation may differ for secondary, nonlinear, CMB features.) For example, after recombination the response of the CMB angular power spectrum  $C_\ell$  to a change of subhorizon potentials is easily quantifiable with eq. (41), derived in the Limber approximation. This response is suppressed relative to the contribution (40) from the horizon entry by a factor  $\frac{r}{\ell\delta\tau}$ . By the arguments of Sec. 5.4.3, for linear changes of subhorizon potentials this factor is much smaller than unity ( $\sim \mathcal{H}/k$ ).

The CMB is an excellent probe of the potentials on the horizon scales at high redshifts. The dark inhomogeneities that enter the horizon at a redshift  $z$  affect most of all the CMB multipoles with  $\ell \sim z/20$  for the radiation epoch and  $\ell \sim 2\sqrt{z}$  for the matter era, eq. (42). With sufficient angular resolution of the detector and reliable subtraction of foregrounds and secondaries, the larger number of statistically-independent multipoles at higher  $\ell$ 's improves the constraints on the parameters that describe the dynamics at higher redshifts ( $z, z + \Delta z$ ) as  $\sqrt{z\Delta z}$  for radiation and  $\sqrt{\Delta z}$  for matter domination, eq. (45).

In contrast, matter transfer functions are more sensitive to the potential  $\Phi$  at low redshifts. The gravitational impact on massive matter at the later times is erased less by the Hubble friction. The response of matter overdensity to  $\Phi(\tau)$  at any past epoch since the horizon entry can be quantified by a simple equation  $\Delta(\delta\rho_m/\rho_m)_{\text{today}} \sim -\tau\Delta\tau k^2 \Phi(\tau)$ , eq. (24). The reduction of the matter sensitivity to early-time dynamics is manifested in the prefactor  $\tau\Delta\tau$ .

### 7.3. Mapping the dark properties

The potentially measurable properties of arbitrary dark sectors may be parameterized by a single function of  $z$  for background and two (transfer) functions of  $z$  and  $k$  for scalar perturbations. The effects of dark sectors or modified gravity on the metric may be phenomenologically described in terms of

$\{\mathcal{H}, \Phi, \Psi\}$ . Assuming the Einstein equations, we may instead consider either dark species' densities and stresses  $\{\rho, \delta^{(c)}, \sigma\}$  or their dynamical characteristics  $\{w, c_{\text{eff}}^2, \sigma\}$  (all reviewed in Sec. 4). The correspondence between the inhomogeneous properties of the dark universe and the observable characteristics of the CMB and LSS is summarized by Table 1 and the text that follows.

### 7.3.1. $\sigma$ vs. $c_{\text{eff}}$

The measurable dynamical characteristics of scalar dark *inhomogeneities* may be fully quantified by the anisotropic stress potential  $\sigma$ , eq. (13), and stiffness (“effective sound speed”)  $c_{\text{eff}}^2$ , Sec. 4.3.

For adiabatic initial conditions, the gravitational potentials  $\Phi(\tau, k)$  and  $\Psi(\tau, k)$  depend on  $c_{\text{eff}}^2$  only at the order  $(k\tau)^2$ , i.e., at a relatively late stage of horizon entry, Sec. 5.2. On the contrary, anisotropic stress of streaming species affects the potentials earlier, already at the order  $(k\tau)^0$ , Sec. 5.1 (Ma & Bertschinger 1995). This distinction may be given the following intuitive illustration: The stiffness affects the motion of the dark species, hence a certain time is required for the dark species to redistribute and start sourcing different potentials. On the other hand, anisotropic stress is generated without displacing the matter. Being itself a source of curvature in the Einstein equations, anisotropic stress changes the gravitational potentials earlier.

There are several observable consequences of the early and late influence respectively of  $\sigma$  and  $c_{\text{eff}}^2$ : Both  $\sigma$  of freely streaming relativistic species and  $c_{\text{eff}}^2$  of a component of dark radiation as stiff as quintessence ( $c_{\text{eff},\phi}^2 = 1$ ) reduce  $\Phi + \Psi$ . Yet the corresponding reductions occur at a different phase of the acoustic CMB oscillations. As a result, the CMB oscillations in the radiation era are somewhat suppressed by the gravitational effect of the anisotropic stress of streaming neutrinos, yet are slightly boosted by the gravitationally coupled perturbations of tracking quintessence, Fig. 1.<sup>21</sup>

Another consequence of the lateness of the gravitational impact of  $c_{\text{eff}}^2$  is a considerably larger ratio of the matter response over the CMB response to a change of  $c_{\text{eff,dark}}^2$ , as compared to this ratio for  $\sigma_{\text{dark}}$ . These results, summarized on the upper half of Table 1, should help distinguish an excess of relic relativistic particles from a subdominant tracking classical scalar field in the radiation era.

### 7.3.2. $c_{\text{eff}}$ vs. $c_p$

Two other potentially observable characteristics of the dark species that should be distinguished from each other are the species'  $c_{\text{eff}}(k)$ , considered above, and the velocity  $c_p$  of the wavefront of their localized perturbation. These quantities need not be functionally related.<sup>22</sup> Together, they are powerful indicators of the nature of dark sectors. For example, interacting relativistic particles whose free-flight time is much smaller than the Hubble time have  $c_{\text{eff}}(k) = c_p = 1/\sqrt{3}$ ; free-streaming rela-

tivistic particles have  $c_{\text{eff}}(k) = 1/\sqrt{3}$  while  $c_p = 1$ ; quintessence is characterized by  $c_{\text{eff}}(k) = c_p = 1$ .

Observationally, the phase of the CMB acoustic oscillations in both temperature and  $E$ -polarization power spectra or their cross-correlation is shifted if and only if  $c_p$  of any of the dark component in the radiation era exceeds the acoustic sound speed  $c_s \simeq 1/\sqrt{3}$ , Sec. 5.3 (Bashinsky & Seljak 2004). Any such dark component contributes to the phase shift by an easily calculable amount. Importantly, the additive shift of the acoustic peaks for adiabatic perturbations is nondegenerate with any of the standard cosmological parameters or with the shape of the primordial power spectrum (Bashinsky & Seljak 2004).

Thus for the robust knowledge of the nature and kinetics of the dark radiation (encompassing neutrinos, possibly other light particles, and early quintessence) both  $c_{\text{eff}}$  and  $c_p$  should be targeted by experimental strategies and data analyses. In particular, the determination of  $c_{\text{eff}}$  appears most promising from the comparison of the *CMB and LSS* power. On the other hand,  $c_p$  is probed increasingly best by the CMB spectra extended toward *higher*  $\ell$ 's, with the *polarization* autocorrelation (EE) being the most crucial (Bashinsky & Seljak 2004).

### 7.3.3. $\Phi$ and $\Phi + \Psi$

We can probe the inhomogeneous properties of the invisible universe more model-independently by constraining metric perturbations directly. Such constraints have a greater validity than general relativity, implied for deducing the dark dynamical properties. They can be placed meaningfully under a weaker assumption of only the visible sectors obeying the equivalence principle, better constrained for them by terrestrial and solar-system probes.

In this perspective, the discussed probes of the scalar component of anisotropic stress  $\sigma$  can be viewed as the direct probes of the difference of the Newtonian-gauge potentials  $\Phi - \Psi$ , eq. (14). The primary anisotropies of the CMB are a sufficiently clean probe of the sum  $\Phi + \Psi$ , entirely responsible for the gravitational driving of the scalar CMB inhomogeneities on all scales and epochs except for a narrow band of redshifts around  $z_{\text{dec}} \sim 1100$ . CDM, on the other hand, responds strictly to the Newtonian potential  $\Phi$  on all scales and at all times, and so does the baryonic matter on large scales after baryon decoupling from the CMB.

Trivially [eq. (7)], the matter growth function is almost directly proportional to past  $\Phi(\tau)$  (as previously noted, weighted by its conformal time  $\tau$ .) The CMB is also affected by the gravitational potentials. Delay of the decay of  $\Phi + \Psi$  after the horizon entry suppresses the CMB power by over an order of magnitude. [In CDM-dominated limit by  $5^2 = 25$  times (Bashinsky 2006) — more than by a factor  $2^2 = 4$  which appears in the apparent description of the Sachs-Wolfe effect in terms of the proper Newtonian perturbations.]

This suppression of the low CMB multipoles is physical: It is absent in models where the metric in the matter era is unperturbed. The suppression is diminished in the models in which the metric is perturbed less than in the  $\Lambda$ CDM scenario. The prominent suppression of the CMB power at  $l \lesssim 100$  by the CDM potential is one of the primary reasons that models without dark matter provide poor fits to the CMB data. The suppression of the CMB temperature anisotropies for  $\ell < 100$  must not be explained as a “resonant self-gravitational driving” of radiation perturbations at  $l \gtrsim 200$ : This effect is caused by and probes the inhomogeneities of matter after equality and not the

<sup>21</sup> The example of tracking quintessence shows that the reduction of the magnitude of dark perturbations *does not necessarily imply* damping of the gravitationally coupled CMB fluctuations, as sometimes stated. The sign of the impact on the CMB anisotropy depends not only on the sign of the change of  $\Phi + \Psi$ , sourced by the dark perturbations, but also the *time* of this change.

<sup>22</sup> Since  $c_{\text{eff}}^2(z, k)$  and  $\sigma(z, k)$  provide the most general parameterization of the observable dynamical properties of the dark perturbations, these functions jointly should encode all the observable signatures of  $c_p$ . Nevertheless, since  $c_p$  has an important kinetic meaning and maps to a sharp non-degenerate signature in the CMB spectra, it is worthwhile to consider this quantity on its own, and to compare it with  $c_{\text{eff}}(k)$ .

TABLE 1

Property	Quantified by	Important for	Effect on the CMB	Effect on Matter
Anisotropic Stress	$\sigma$ , eq. (13) [ $\Phi - \Psi$ , eq. (14)]	Early stage of horizon entry	Amplitude (Suppressed by $\sigma$ from streaming)	Minor on power (Enhanced by $\sigma$ from streaming)
Stiffness	$c_{\text{eff}}^2$ , eq. (15)	Late stage of horizon entry	Amplitude (Enhanced by tracking quintessence)	Medium on power (Suppressed by tracking quintessence)
Velocity of a perturbation front	$c_p$ , Sec. 5.3	Features local in real space	Phase of the acoustic peaks	Phase of baryonic oscillations
Self-clustering	$\Phi, \Phi + \Psi$ eq. (3)	Horizon entry (CMB) and subhorizon evolution (LSS)	Significant suppression of the amplitude	Primary driving of the structure growth

NOTE.—Summary of the discussed properties of the dark sectors, the epochs of their observational relevance, and their effects on the CMB power spectra and on large-scale structure.

inhomogeneities of radiation before equality.

The suppression of  $C_\ell$  for  $\ell \lesssim 100$  severely restricts the alternatives to CDM and the models of dark energy which reduce metric perturbations at any redshift in the matter era. Examples of such mechanisms are contribution of quintessence to the density in the matter era, interaction or unification of dark matter and dark energy (e.g., Wetterich 1988; Perrotta & Baccigalupi 2002; G. R. Farrar, P. J. Peebles 2004; Catena et al. 2004; Scherrer 2004), or MOND-inspired alternatives to dark-matter (Milgrom 1983; Bekenstein 2004).

#### 7.4. Modified gravity

Many authors have suggested that modification of general relativity on cosmological scales is the cause of the cosmic acceleration (for recent reviews see Copeland et al. 2006; Nojiri & Odintsov 2007) or even of the apparent manifestations of dark matter (Milgrom 1983; Bekenstein 2004). In Sec. 6 we consider the phenomenology of typical models of modified gravity (MG) that retain the equivalence principle for the visible sectors. We show that in these models all gravitational impact of the hidden physics can be described within the same parameterization schemes of Sec. 4, developed to quantify the observable properties of dark sectors that are coupled by general relativity (GR). Indeed, these schemes were restricted only by the covariance of the visible dynamics, the assumption of the Einstein equations, and the local conservation of the dark energy and momentum. However, for any covariant visible dynamics, the formal dark energy-momentum tensor (46) that is missing in the Einstein equations is covariantly conserved automatically (Sec. 6). Thus all observable signatures of MG can be mimicked by effective dark energy and momentum that influence the visible species according to the Einstein equations and during evolution are conserved locally.

Particularly, the nonstandard structure growth or  $\Phi/\Psi$  ratio that are predicted by *any* MG model of the considered broad class can in principle be reproduced without violation of the Einstein equations by sufficiently peculiar dark dynamics. Nevertheless, first, such signatures would still signal some non-

minimal physics and therefore should be considered for experimental constraints whenever possible. Second, GR remains falsifiable by other effects; in particular, by the violation of the equivalence principle by apparent dark dynamics. This may be manifested in the strong dependence of the dark dynamics on the visible matter (Sec. 6.1), and in the signatures of effective or real superluminal dark flows (e.g., Sec. 6.2). GR can also be falsified by nonstandard phenomenology of gravitational waves (e.g. Kahya & Woodard 2007, and Secs. 6.2 and 6.3).

#### ACKNOWLEDGMENTS

I am grateful to Salman Habib and Katrin Heitmann for valuable discussions, suggestions, and comments on the manuscript. I thank Daniel Holz and Gerry Jungman for stimulating talks and useful suggestions. This work was supported by the US Department of Energy via the LDRD program of Los Alamos.

#### APPENDIX

##### CMB SENSITIVITY TO $\delta\Phi$ ON SMALL SCALES

We quantify the CMB sensitivity to the metric inhomogeneities on subhorizon scales and at late times using the Limber approximation (Limber 1954), applied to the CMB by Kaiser (1984, 1992) and Hu & White (1996). The Limber approximation for the CMB power spectrum  $C_l$  assumes that the change of the source  $S$  in the line-of-sight integral (31) is negligible over the wavelength of a typical contributing mode  $k^{-1} \sim r/\ell$ . If  $\delta\tau$  is a temporal scale over which the source changes by an order of unity then the above condition is equivalent to  $k\delta\tau \gg 1$ . In the Limber limit,  $C_l$  is primarily contributed by the modes with  $|\mathbf{k} \cdot \mathbf{n}| \delta\tau \lesssim 1$ , while positive and negative contributions to  $\Delta T/T$  from the peaks and troughs of the other modes cancel (Hu & White 1996).

The ISW contribution to the anisotropy source (32) is

$$S_{\text{ISW}} = g(\dot{\Phi} + \dot{\Psi}). \quad (\text{A1})$$

This direction-independent source in the Limber approximation gives the following additive contribution to the power spectrum (Kaiser 1992; Hu 2000):

$$\delta C_\ell \approx \frac{2\pi^2}{\ell^3} \int dr r \Delta_{\text{ISW}}^2(k = \ell/r), \quad (\text{A2})$$

where  $\Delta_{\text{ISW}}^2(k) \equiv k^3 P_{\text{ISW}}(k)/(2\pi^2)$  is the dimensionless power spectrum of  $S_{\text{ISW}}(\mathbf{k})$ , evaluated at a time  $\tau(r)$ . Thus the ISW contribution is

$$\delta C_\ell \approx \frac{2\pi^2}{\ell^3} \int dr r g^2 (\dot{\Phi} + \dot{\Psi})^2 \Delta_\zeta^2(k = \ell/r), \quad (\text{A3})$$

where  $\Phi$  and  $\Psi$  now denote the potentials' transfer functions, i.e., the potentials in the perturbation modes that are normalized to a unit primordial curvature perturbation,  $\zeta_{\text{in}}(\mathbf{k}) \equiv 1$ .

We now quantify the sensitivity of the power spectrum to a change of the potential  $\delta\Phi$  on subhorizon scales over a time interval  $\delta\tau \gg r/\ell$ . For an estimate, in eq. (A3) we set  $g \approx 1$  at the considered late times, neglect the variation of  $\Delta_\zeta^2(\ell/r)$  for the nearly scale-invariant primordial power, and evaluate the remaining integral as

$$\int dr r (\dot{\Phi} + \dot{\Psi})^2 \sim r \frac{[\delta(\Phi + \Psi)]^2}{\delta\tau}.$$

Then

$$\delta C_\ell \sim \frac{2\pi^2 \Delta_\zeta^2(\ell/r)}{\ell^2} [\delta(\Phi + \Psi)]^2 \frac{r}{\ell \delta\tau}. \quad (\text{A4})$$

#### REFERENCES

- Armendariz-Picon, C., Mukhanov, V. F., & Steinhardt, P. J. 2001, *Phys. Rev.*, D63, 103510
- Baccigalupi, C. 1999, *Phys. Rev. D*, 59, 123004
- Baccigalupi, C. & Perrotta, F. 2000, *MNRAS*, 314, 1
- Bardeen, J. M. 1980, *Phys. Rev. D*, 22, 1882
- Bardeen, J. M., Steinhardt, P. J., & Turner, M. S. 1983, *Phys. Rev. D*, 28, 679
- Bashinsky, S. 2004, *astro-ph/0411013*
- , 2005, *astro-ph/0505502*
- , 2006, *Phys. Rev.*, D74, 043007
- Bashinsky, S. & Bertschinger, E. 2001, *Physical Review Letters*, 87, 81301
- , 2002, *Phys. Rev. D*, 65, 123008
- Bashinsky, S. & Seljak, U. 2004, *Phys. Rev.*, D69, 083002
- Beacom, J. F., Bell, N. F., & Dodelson, S. 2004, *Phys. Rev. Lett.*, 93, 121302
- Bekenstein, J. D. 2004, *Phys. Rev.*, D70, 083509
- Bell, N. F., Pierpaoli, E., & Sigurdson, K. 2006, *Phys. Rev.*, D73, 063523
- Bertschinger, E. 2006, *Astrophys. J.*, 648, 797
- Blumenthal, G. R., Pagels, H., & Primack, J. R. 1982, *Nature*, 299, 37
- Bowen, R., Hansen, S. H., Melchiorri, A., Silk, J., & Trotta, R. 2002, *MNRAS*, 334, 760
- Bradac, M. et al. 2006, *Astrophys. J.*, 652, 937
- Carlson, E. D., Machacek, M. E., & Hall, L. J. 1992, *ApJ*, 398, 43
- Catena, R., Fornengo, N., Masiero, A., Pietroni, M., & Rosati, F. 2004, *Phys. Rev.*, D70, 063519
- Chacko, Z., Hall, L. J., Okui, T., & Oliver, S. J. 2004, *Phys. Rev.*, D70, 085008
- Chacko, Z., Hall, L. J., Oliver, S. J., & Perelstein, M. 2005, *Phys. Rev. Lett.*, 94, 111801
- Chandrasekhar, S. 1960, *Radiative transfer* (New York: Dover, 1960)
- Chiba, T. & Takahashi, R. 2007, *Phys. Rev.*, D75, 101301
- Cirelli, M. & Strumia, A. 2006, *JCAP*, 0612, 013
- Clowe, D., Bradač, M., Gonzalez, A. H., Markevitch, M., Randall, S. W., Jones, C., & Zaritsky, D. 2006, *ApJ*, 648, L109
- Copeland, E. J., Sami, M., & Tsujikawa, S. 2006, *Int. J. Mod. Phys.*, D15, 1753
- de Laix, A. A., Scherrer, R. J., & Schaefer, R. K. 1995, *Astrophys. J.*, 452, 495
- Dodelson, S. & Liguori, M. 2006, *Phys. Rev. Lett.*, 97, 231301
- Durrer, R. 1990, *Phys. Rev.*, D42, 2533
- , 1994, *Fund. Cosmic Phys.*, 15, 209
- , 2001, *J. Phys. Stud.*, 5, 177
- Dvali, G. R., Gabadadze, G., & Porrati, M. 2000, *Phys. Lett.*, B485, 208
- Eisenstein, D. J. et al. 2005, *Astrophys. J.*, 633, 560
- Erickson, J. K., Caldwell, R. R., Steinhardt, P. J., Armendariz-Picon, C., & Mukhanov, V. F. 2002, *Phys. Rev. Lett.*, 88, 121301
- Fardon, R., Nelson, A. E., & Weiner, N. 2006, *JHEP*, 03, 042
- G. R. Farrar, P. J. Peebles. 2004, *Astrophys. J.*, 604, 1
- Grossman, Y., Kilic, C., Thaler, J., & Walker, D. G. E. 2005, *Phys. Rev.*, D72, 125001
- Hannestad, S. 2005, *JCAP*, 0502, 011
- Hannestad, S. & Raffelt, G. G. 2006, *JCAP*, 0611, 016
- Hinshaw, G. et al. 2006, *astro-ph/0603451*
- Hu, W. 1998, *Astrophys. J.*, 506, 485
- , 2000, *Astrophys. J.*, 529, 12
- Hu, W., Eisenstein, D. J., Tegmark, M., & White, M. J. 1999, *Phys. Rev.*, D59, 023512
- Hu, W. & Okamoto, T. 2002, *Astrophys. J.*, 574, 566
- Hu, W. & Sugiyama, N. 1994, *Phys. Rev.*, D50, 627
- , 1995, *Phys. Rev.*, D51, 2599
- Hu, W. & Sugiyama, N. 1996, *ApJ*, 471, 542
- Hu, W., Sugiyama, N., & Silk, J. 1997, *Nature*, 386, 37
- Hu, W. & White, M. J. 1996, *Astron. Astrophys.*, 315, 33
- Ishak, M., Upadhye, A., & Spergel, D. N. 2006, *Phys. Rev.*, D74, 043513
- Kahya, E. O. & Woodard, R. P. 2007, *arXiv:0705.0153* [astro-ph]
- Kaiser, N. 1983, *MNRAS*, 202, 1169
- , 1984, *ApJ*, 282, 374
- Kaiser, N. 1992, *Astrophys. J.*, 388, 272
- Kamionkowski, M., Kosowsky, A., & Stebbins, A. 1997, *Phys. Rev. Lett.*, 78, 2058
- Kendall, M. & Stuart, A. 1979, *The advanced theory of statistics. Vol.2: Inference and relationship* (London: Griffin, 1979, 4th ed.)
- Knox, L. 1995, *Phys. Rev.*, D52, 4307
- Knox, L., Song, Y.-S., & Tyson, J. A. 2005, *astro-ph/0503644*
- Kodama, H. & Sasaki, M. 1984, *Prog. Theor. Phys. Suppl.*, 78, 1
- , 1986, *Int. J. Mod. Phys.*, A1, 265
- Kunz, M. & Sapone, D. 2007, *Phys. Rev. Lett.*, 98, 121301
- Landau, L. D. & Lifshitz, E. M. 1975, *The classical theory of fields* (Course of theoretical physics, Vol. II - Oxford, Pergamon Press, 1975)
- Limber, D. N. 1954, *ApJ*, 119, 655
- Linde, A. & Mukhanov, V. 2006, *JCAP*, 0604, 009
- Linder, E. V. 2005, *Phys. Rev.*, D72, 043529
- Lopez, R. E., Dodelson, S., Heckler, A., & Turner, M. S. 1999, *Phys. Rev. Lett.*, 82, 3952
- Ma, C. & Bertschinger, E. 1995, *ApJ*, 455, 7
- Magueijo, J. C. R. 1992, *Phys. Rev.*, D46, 3360
- Markevitch, M. et al. 2004, *Astrophys. J.*, 606, 819
- Milgrom, M. 1983, *ApJ*, 270, 365
- Mukhanov, V. F., Feldman, H. A., & Brandenberger, R. H. 1992, *Phys. Rept.*, 215, 203
- Nojiri, S. & Odintsov, S. D. 2007, *Int. J. Geom. Meth. Mod. Phys.*, 4, 115
- Okui, T. 2005, *JHEP*, 09, 017
- Olive, K. A. & Turner, M. S. 1982, *Phys. Rev.*, D25, 213
- P. Ferreira, M. Joyce. 1997, *Phys. Rev. Lett.*, 79, 4740
- Page, L. et al. 2006, *astro-ph/0603450*
- Perotto, L., Lesgourgues, J., Hannestad, S., Tu, H., & Wong, Y. Y. Y. 2006, *JCAP*, 0610, 013
- Perrotta, F. & Baccigalupi, C. 2002, *Phys. Rev.*, D65, 123505
- Press, W. H. & Vishniac, E. T. 1980, *Astrophys. J.*, 239, 1
- R. K. Sachs, A. M. Wolfe. 1967, *Astrophys. J.*, 147, 73
- Ratra, B. & Peebles, P. J. 1988, *Phys. Rev.*, D37, 3406
- Scherrer, R. J. 2004, *Phys. Rev. Lett.*, 93, 011301
- Seljak, U. 1996, *astro-ph/9608131*
- Seljak, U., Slosar, A., & McDonald, P. 2006, *JCAP*, 0610, 014
- Seljak, U. & Zaldarriaga, M. 1996, *Astrophys. J.*, 469, 437
- , 1997, *Phys. Rev. Lett.*, 78, 2054
- , 1999, *Phys. Rev.*, D60, 043504
- Silk, J. 1968, *Astrophys. J.*, 151, 459
- Skordis, C., Mota, D. F., Ferreira, P. G., & Boehm, C. 2006, *Phys. Rev. Lett.*, 96, 011301
- Spergel, D. N. & Steinhardt, P. J. 2000, *Phys. Rev. Lett.*, 84, 3760
- Spergel, D. N. et al. 2006, *astro-ph/0603449*
- Tegmark, M. et al. 2004, *Astrophys. J.*, 606, 702
- , 2006, *Phys. Rev.*, D74, 123507
- Wands, D., Malik, K. A., Lyth, D. H., & Liddle, A. R. 2000, *Phys. Rev. D*, 62, 43527
- Weinberg, S. 2002, *Astrophys. J.*, 581, 810
- , 2004, *Phys. Rev.*, D69, 023503
- Wetterich, C. 1988, *Nucl. Phys.*, B302, 668
- Zaldarriaga, M., Spergel, D. N., & Seljak, U. 1997, *Astrophys. J.*, 488, 1
- Zlatev, I., Wang, L.-M., & Steinhardt, P. J. 1999, *Phys. Rev. Lett.*, 82, 896